Manawatū-Whanganui Region Catchment Nitrogen Models

Supporting Regional Plan Change 2

July 2020

Prepared By:

Ton Snelder

Tim Cox*

Tim Kerr

Caroline Fraser

Stephen Collins¥

*Streamlined Environmental Ltd

¥ Horizons Regional Council

For any information regarding this report please contact:

Ton Snelder

Phone: 0275758888

Email: ton@lwp.nz

LWP Ltd

PO Box 70

Lyttelton 8092

New Zealand

Quality Assurance Statement

Version	Reviewed By	
Final	Ngaire Phillips*	

Table of Contents

Executive Summary

Catchment water quality models were developed for the four major river basins in the Horizons Region: the Manawatū (including the Horowhenua and Coastal Tararua catchments), the Rangitikei, the Whanganui, and the Whangaehu (including the Turakina River catchment). The entire Manawatū- Whanganui region is encapsulated by the four models. The models use sub-catchment export and attenuation coefficients and point source load estimates to simulate the generation, transport, and downstream delivery of total nitrogen (TN) loads throughout the region. The models were developed to investigate the impact of regulating nitrogen discharge allowances from intensively farmed land throughout the region. It is anticipated that the models will be used to estimate loads and concentrations under a range of potential management scenarios.

A satisfactory calibration was achieved for all four basin models. Downstream calibration targets (observed TN loads) were all achieved with sensible adjustments to upstream attenuation coefficients, within expected ranges, and, in a limited number of cases, minor adjustments to independently derived export coefficients. Patterns of attenuation within, and between, basins have been noted but not yet fully explained.

Models are uncertain, and the uncertainty of the key model parameters (the attenuation coefficients) have been demonstrated in this report. This uncertainty is largely unavoidable and results from uncertainty in the water quality station TN loads and estimated sub-catchment TN export coefficients. This uncertainty needs to be considered when using the models to make predictions of TN loads and concentrations under different management scenarios. The estimated loads and concentrations in absolute terms should be regarded as less certain than the relative difference in loads and concentrations between locations and scenarios.

1   Introduction

Horizons Regional Council (HRC) has proposed a change to its Regional Policy Statement and Regional Plan (the One Plan) known as Plan Change 2. Proposed Plan Change 2 is focused on the One Plan's provisions that manage nutrient loss from existing intensive farming land uses (dairy farming, commercial vegetable growing, cropping, and intensive sheep and beef) in target water management sub-zones. These provisions are no longer working as intended when the One Plan was developed. Proposed Plan Change 2 will update the cumulative nitrogen leaching maximums in the One Plan Table 14.2 to reflect improvements in the nutrient modelling software tool Overseer; reinforce good management practices as part of intensive farming land use activities; and provide a workable pathway for landowners to apply for resource consent for intensive farming land use activities that cannot achieve Table 14.2 cumulative leaching maximums.

Proposed Plan Change 2 will have effects on instream loads and concentrations of nitrogen across the Manawatū-Whanganui Region. These effects will be spatially variable for two reasons. First, land use changes resulting from Proposed Plan Change 2 will not be evenly distributed across the region meaning that future land use intensity will vary between the region's catchments. Second, there is environmentally mediated variation in both potential nitrogen losses from land use and the processing of nitrogen (attenuation) as it moves through the drainage network. Because these two factors interact, the water quality outcomes of proposed Plan Change 2 are complex and their assessment requires catchment water quality modelling. This report describes the development and calibration of catchment water quality models for the purpose of assessing the impacts of the plan change on in-stream nitrogen loads and concentrations across the region. This report does not describe the use of the models to assess impacts; this will be the subject of other documentation.

Catchment water quality models were developed for the Manawatū-Whanganui region's four major river basins: the Manawatū (including the Horowhenua and Coastal Tararua catchments), the Rangitikei, the Whanganui, and the Whangaehu (including the Turakina River catchment). The entire region is encapsulated by the four models. The models use sub-catchment export and attenuation coefficients to simulate the generation, transport, and downstream delivery of total nitrogen (TN) loads throughout the region. The models can be used to investigate the potential effects of nitrogen discharge from land (diffuse source discharges) and point source discharges. The models can also be used to assess the effects of differing discharge standards throughout the region and to test the effectiveness and feasibility of mitigations. The models were developed in a usable framework to allow for future application by a range of potential end users. In future use of the models, the primary input will be scenario assumptions about land use and nitrogen loss rates, and the primary outputs will be loads and concentrations at reporting locations distributed across throughout the river network.

2   Water quality models

2.1   Model software

The Horizon models were developed using Streamlined Environmental Limited's (SEL) Contaminant Allocation and Simulation Model (CASM) software. CASM is designed as a flexible, and usable, generalized modelling tool for simulating diffuse and point source contamination at a catchment scale.

CASM calculates the generation of a range of user-defined contaminants at a catchment scale and the fate and transport of the contaminants through the catchment's dendritic stream network. Contaminant sources are represented in the model as individual nodes, discharging to specific streams of any order. Contaminant sources can be either diffuse (e.g. farms) or point (e.g. municipal discharges). Sources can be aggregated for lower resolution models, including to a sub-catchment scale, or explicitly represented as individual property nodes for higher resolution models. Diffuse source contamination calculations follow the widely used "export coefficient" approach, with prescribed areal average mass loading rates (kg ha^{-1} yr^{-1}) linked to land use categories. Point source loading rates are simply user defined for each node. Both diffuse and point source loading parameters can be prescribed as seasonally variable in CASM.

Three forms of contaminant attenuation are available in the model: diffuse pathway, instream, and reservoir. The first is applicable for diffuse sources only and represents potential mass losses occurring from the point of export or leaching to the point of discharge to the receiving stream. The second captures attenuation that may occur during downstream transport within the stream channel (e.g. due to settling, uptake, or transformation). The third provides for additional enhanced attenuation that may occur in intercepting reservoirs as a function of residence time. Like the source terms described above, all attenuation parameters can be defined seasonally in the model.

Note that, for the models described here, only diffuse pathway attenuation is included, except for two short reaches in the Manawatū River basin. Both export coefficients and attenuation coefficients are prescribed on an annual average basis. Parameter seasonality is not included in the current models. Additionally, no reservoirs are explicitly included in any of the models.

Any number of water quality "stations" can be defined in the model at any instream location. These model objects provide for output summaries specific to the given location. These summaries include total contaminant loads (kg/month), concentration (mg/L), and source tracking (a breakdown of contributing upstream sources). Instream target concentrations can also be prescribed at these stations for reference, or to trigger mitigation optimization calculations (described below).

The CASM software offers three modes of simulation: deterministic, stochastic, and optimization. Deterministic simulations involve the tracking of contaminant mass from point of export (diffuse) or discharge (point) through a dendritic stream network to a series of downstream monitoring stations. The model varies source loading seasonally, combines loads at appropriate locations, and attenuates the loads based on user-defined parameters, providing for time-varying loads (and/or concentrations) at any location in the modelled catchment. The model also provides useful source tracking output, showing relative contributions of load from upstream categories of diffuse and point sources. Up to five (5) different user-defined contaminants can be simulated in a single model run.

Stochastic simulations allow the user to perform a comprehensive uncertainty analysis for their constructed model and to frame model predictions in the form of highly useful probability distributions. Rather than single value outputs of modelled river concentrations, stochastic simulations present these outputs in terms of exceedance probabilities (or "risk"). For stochastic simulations, simple probability distributions can be defined for any combination of the following key model inputs: export coefficients, diffuse pathway attenuation coefficients, and instream attenuation coefficients. Optimization simulations perform the same fate and transport calculations as in deterministic and stochastic simulations but also provide an optimal mitigation strategy to achieve prescribed downstream water quality concentration

targets. Optimality is determined in the model based on user-defined mitigation cost tables associated with each source node. Note that only the deterministic mode of simulation was used for the modelling described here.

2.2   Model response, calibration date, basins and sub-catchments

Previous investigations of nitrogen attenuation in the region have considered soluble inorganic nitrogen (SIN) rather than TN (Collins *et al.*, 2017). In this study, the model response was TN loads, rather than SIN, because diffuse source nitrogen losses from farms are expressed in terms of TN, including the loss rates defined in the One Plan Table 14.2.

The calibration year was 2012. This year was chosen because it was prior to implementation of the One Plan provisions for management of nitrogen discharges to land. Therefore, 2012 was prior to regulation of intensive farming land use (IFLU) in the region applying Table 14.2. The calibrated model therefore represents the pre-regulation baseline and enables us to model changes in water quality as a result of implementation of both the operative and proposed One Plan nutrient management provisions.

Each river basin model was subdivided into sub-catchments based on HRC's Water Management Zones (WMZ; Table 1). Each WMZ is represented in one of the four models (Figures 1 – 4).

Table 1. High-level summary of each of the four constructed models

Model characteristics	Manawatū River	Rangitikei River	Whanganui River	Whangaehu River
Total drainage area (ha)	733,600	401,500	750,400	312,800
Number of WMZ sub-catchments	50	15	32	15
Total number of diffuse nodes	1425	354	678	327
Number of point sources	22	8	2	5
Number of WQ calibration points	31	7	6	6
Number of explicit tributaries	28	8	12	7
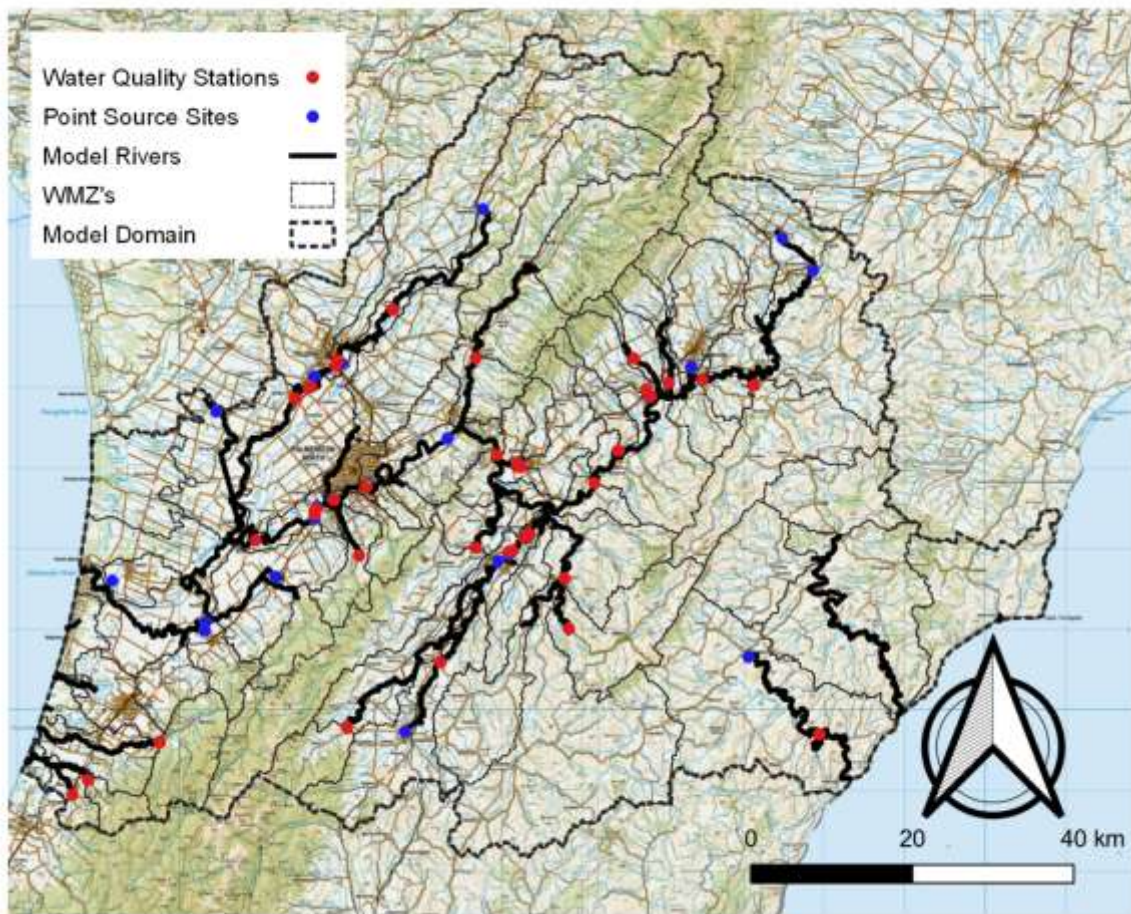
Figure 1. Map showing the Manawatū River basin model domain and spatial subdivision by WMZs. Note that this model includes the Horowhenua and Coastal Tararua catchments.The red points indicate the water quality stations and the blue points indicate the point sources.
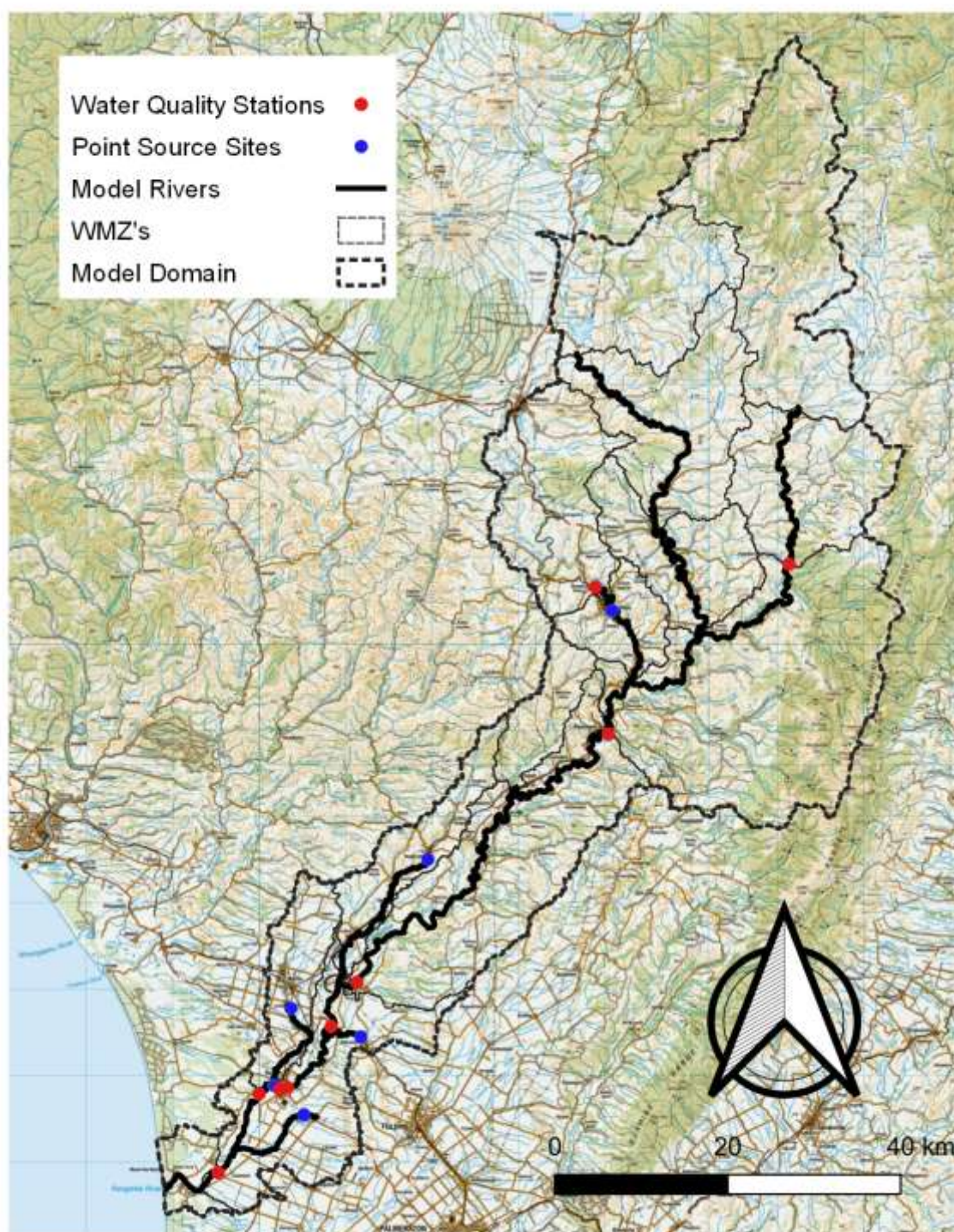
Figure 2. Map showing the Rangitikei River basin model domain and spatial subdivision by WMZs.The red points indicate the water quality stations and the blue points indicate the point sources.
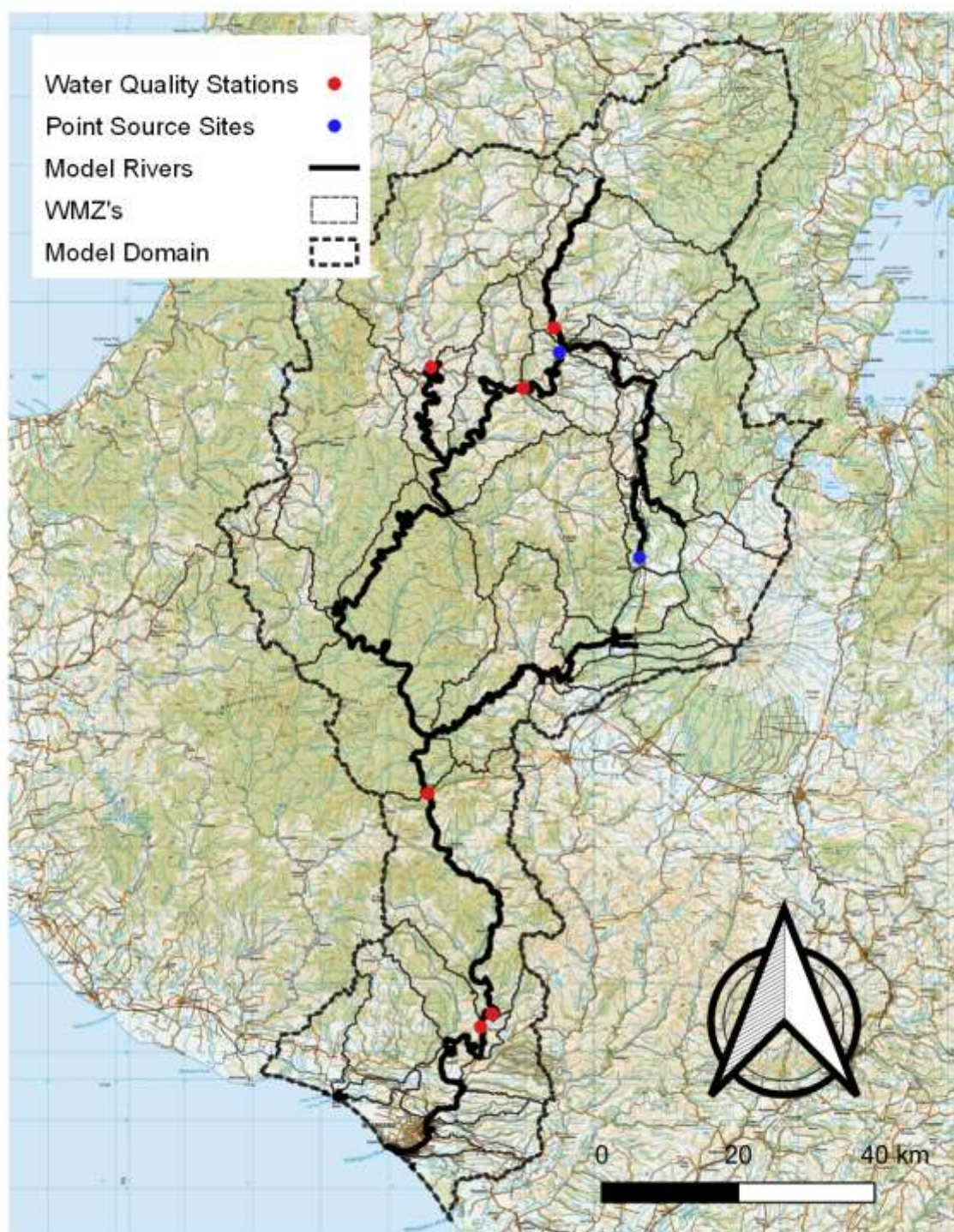
Figure 3. Map showing the Whanganui River basin model domain and spatial subdivision by WMZs. The red points indicate the water quality stations and the blue points indicate the point sources.
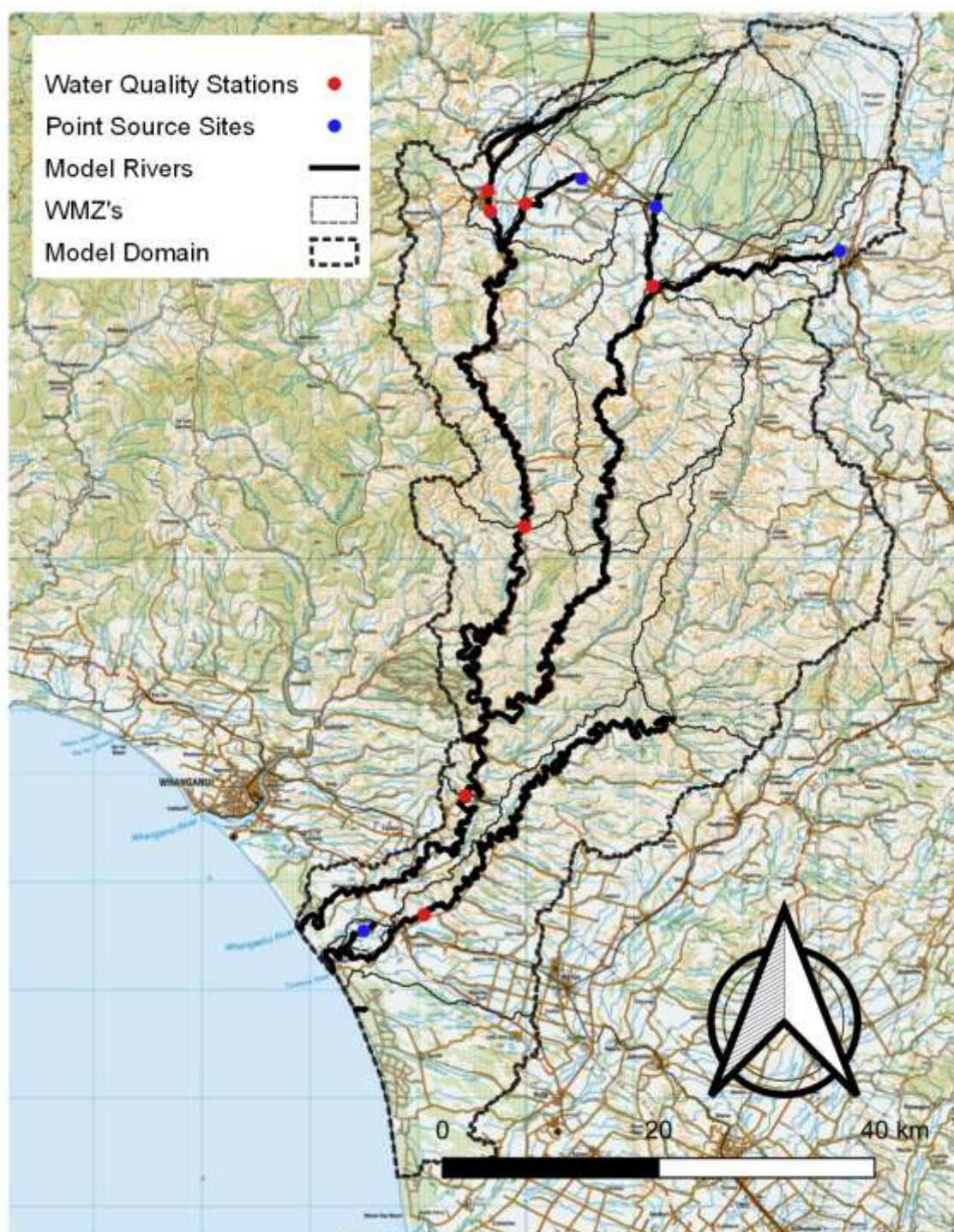
Figure 4. Map showing the Whangaehu River basin model domain and spatial subdivision by WMZs. Note that this includes both the Whangaehu and Turakina Rivers and their catchments.The red points indicate the water quality stations and the blue points indicate the point sources.

2.3   Water quality station loads

Estimates of mean annual loads of TN at 60 water quality stations in 2012 (i.e., the baseline year) were derived from monthly TN concentrations and observed or modelled daily flows (Figure 1 to 4). Details of the load calculation methods are provided in Appendix A and further details are contained in Fraser and Snelder (2019). The locations and magnitudes of the loads (as export coefficients kg N ha^{-1} yr^{-1}) at the water quality stations are shown in Figure 5.

Export Coefficient (kg TN ha^{-1} yr^{-1})   ◆ 5   ◆ 10   ◆ 15
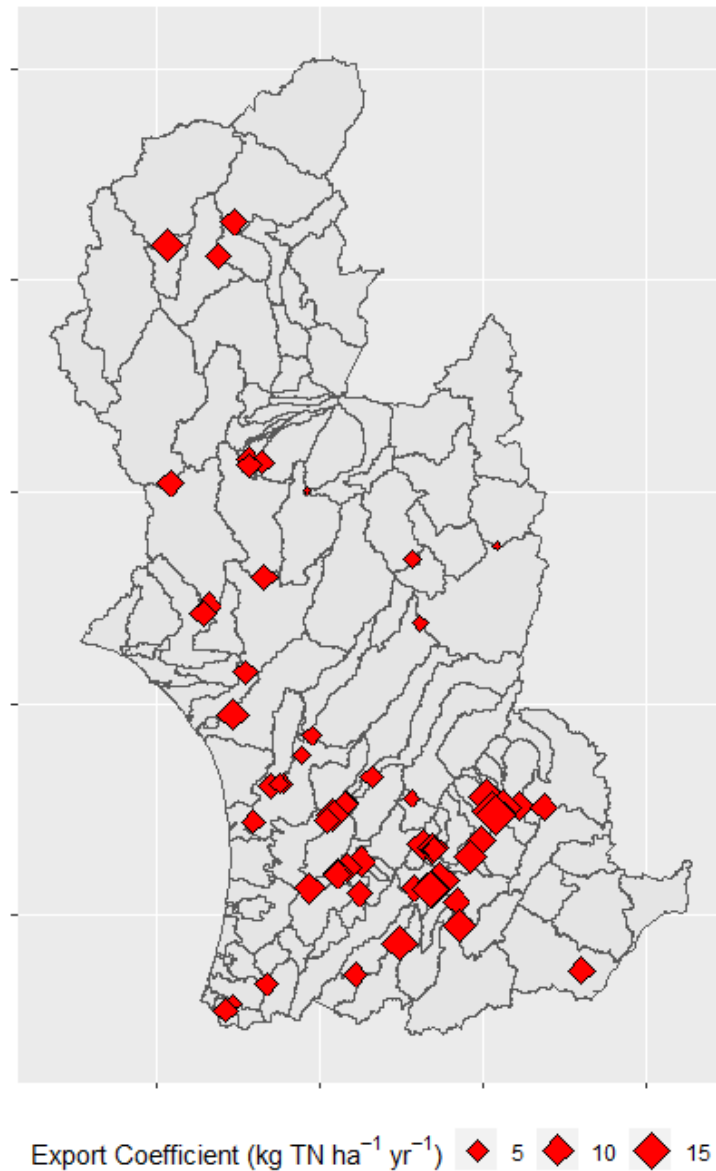
Figure 5. Location and loads (kg TN ha^{-1} yr^{-1}) at 60 water quality monitoring stations that were included in the models.

2.4   Point source discharges

The estimated mean annual loads of TN discharged in 2012 (i.e., the baseline year) at 37 consented discharges > 20m^3 d^{-1} across the region are shown Figure 6. Data describing discharge concentration of TN for these point source discharges were provided by HRC. The point source loads comprised consented discharges that were operating at any time during the period 2007-2017. Discharge volume estimates were provided by HRC (mean daily flows, based on consented volumes and/or spot observations). Mean concentrations were calculated based on continuous or sporadic monitoring records for these discharges. A summary of the estimated discharges in 2012 (i.e., the baseline year) and 2017 are provided in Appendix B (more details are provided in Fraser and Snelder (2019).
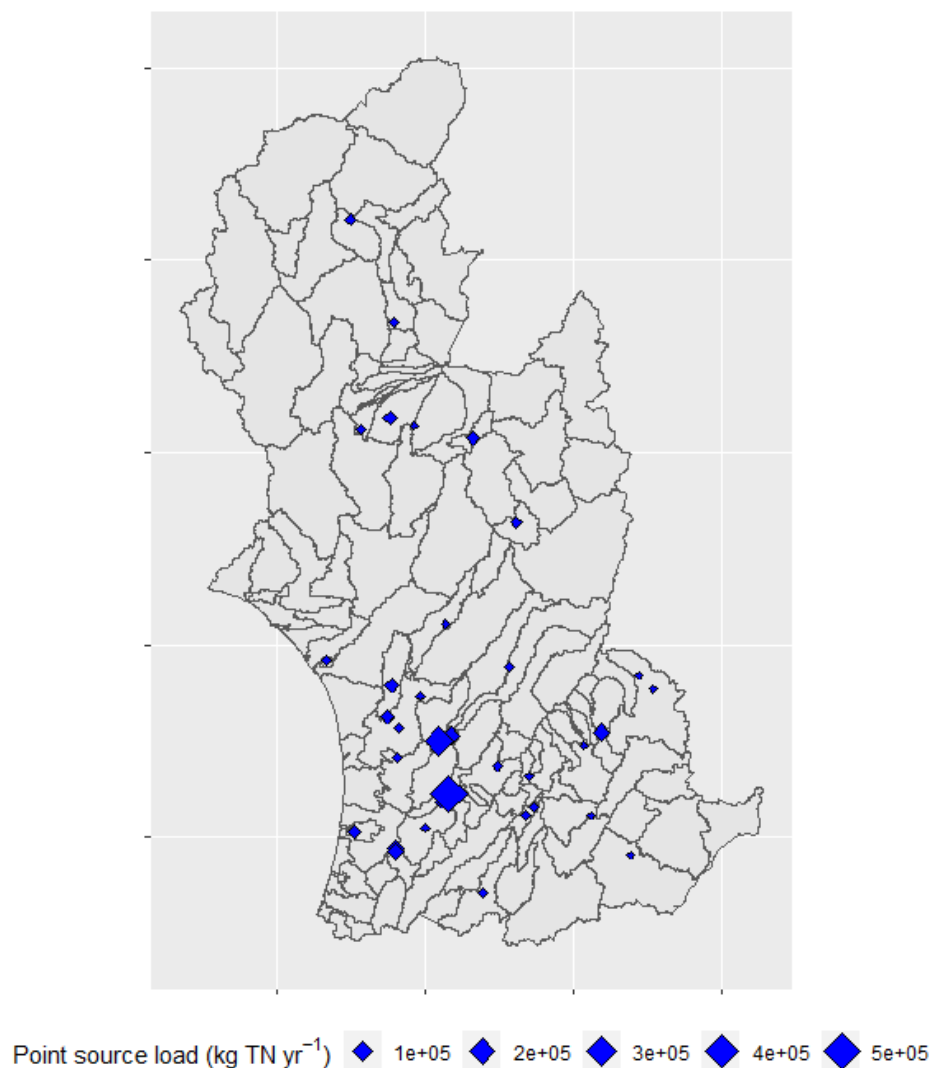
Figure 6. Location and estimated loads (kg TN yr^{-1}) in 2012 of 37 consented point-source discharges that were included in the models.

2.5 Land use and diffuse source nitrogen export coefficients

2.5.1 Land use map and changes in land use intensity

At the time of reporting, the best available land use data representing the baseline year (2012) was HRC's 2008 land use map, which describes regional variation in land use in nine categories (Figure 7). The non-congruence of the land use map and the catchment nitrogen emission estimates that were used to calibrate the model is unlikely to be statistically significant (i.e., any differences resulting from changes in land use between 2008 and 2012 would be within the model uncertainty). A detailed discussion of the implications of the mismatch between the land use map and baseline year is provided in Appendix C.

2.5.2 Export coefficients

We used export coefficients based on Bright *et al.* (2018). Bright *et al.* (2018) provided estimates of nitrogen diffuse source export coefficients under the same nine land use categories shown on Figure 7, which apply New Zealand wide. For each land use category, the export coefficients defined by Bright *et al.* (2018) account for variation in export coefficients based on a classification defined by defined by four biophysical factors including: climate zone, plant available soil water capacity (PAW), and whether the land is irrigable and irrigated. Variation in these factors is captured by a small number of categories for each factor. Within the Manawatū-Whanganui Region, there are five climate zones, and three PAW categories (35mm, 60mm, 120mm). The factors irrigable and irrigated are binary and we use "Y" or "N" to discriminate irrigable from non-irrigable land and "Irrigated" and "Dryland" to discriminate irrigation status. Details concerning these natural and land use characteristics, and some adjustments to Bright *et al.'s* (2018) export coefficients to account for regionally specific conditions and information, are provided below.

Variation in climate was based on the NZ Meteorological Service Climate Regions map (NZMS 315/2) following modifications that were made and described by Bright *et al.* (2018; Figure 8).
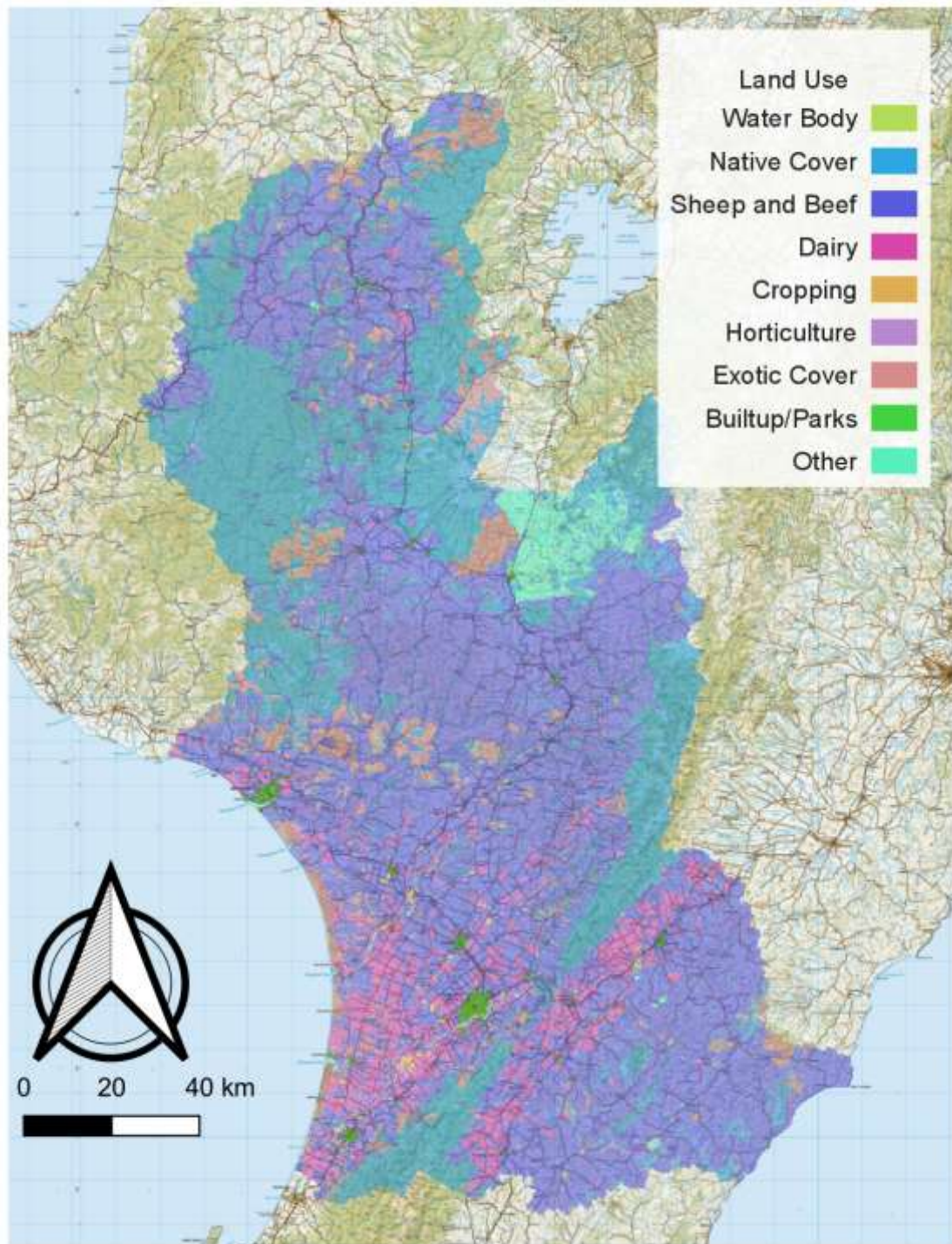
Figure 7. Land use map representing 9 land use/cover categories. This map represents land use in 2008. Note that horticultural land cover is very difficult to distinguish at this scale due to the small area of properties.
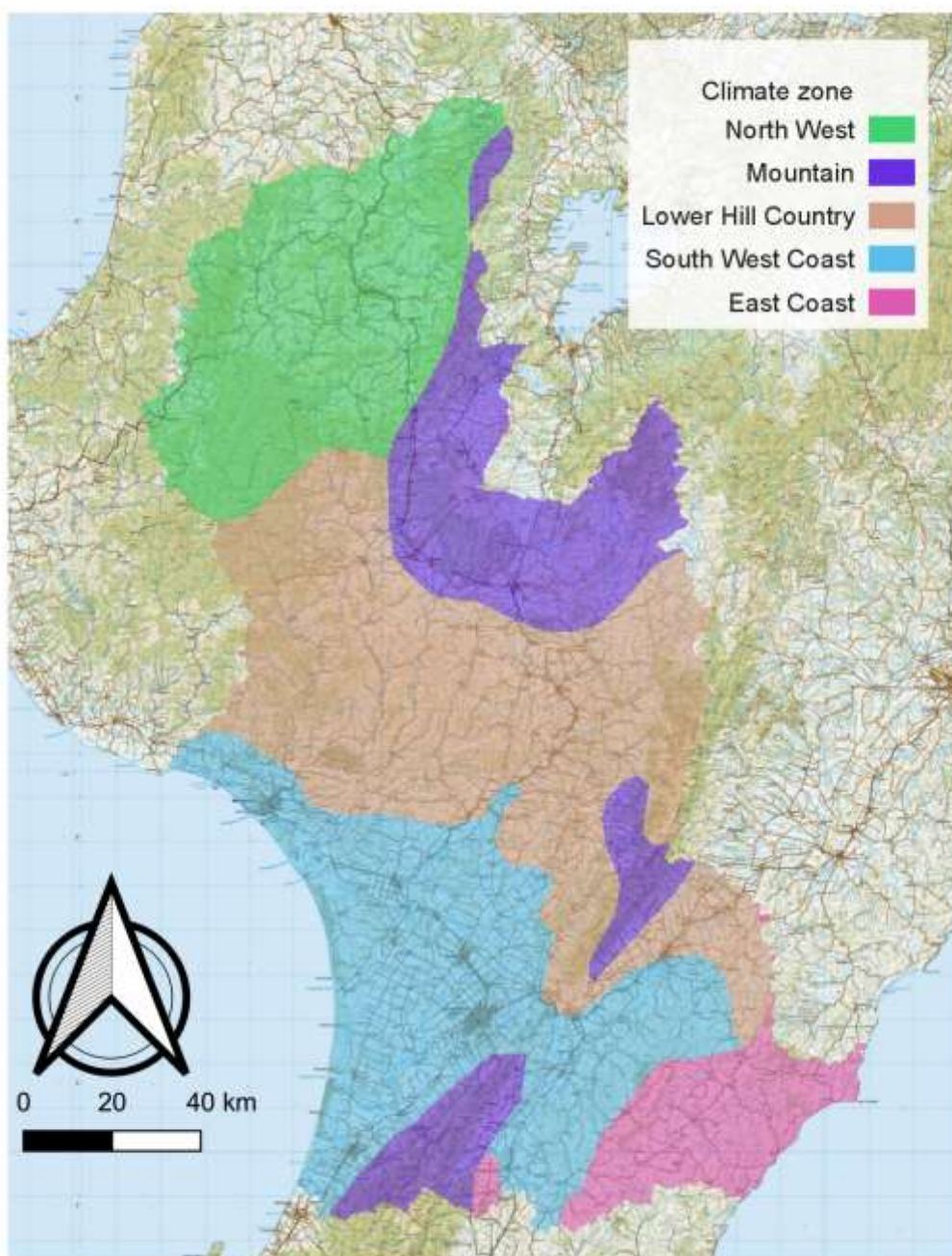
Figure 8. Climate variation described using five different categories.

Variation in soils described by the PAW was obtained from the fundamental soils layer (Figure 9). The FSL is described in https://soils.landcareresearch.co.nz/soil-data/fundamental-soil-layers and the PAW dataset used in this modelling is available at https://lris.scinfo.org.nz/layer/100-fsl-profile-available-water/.
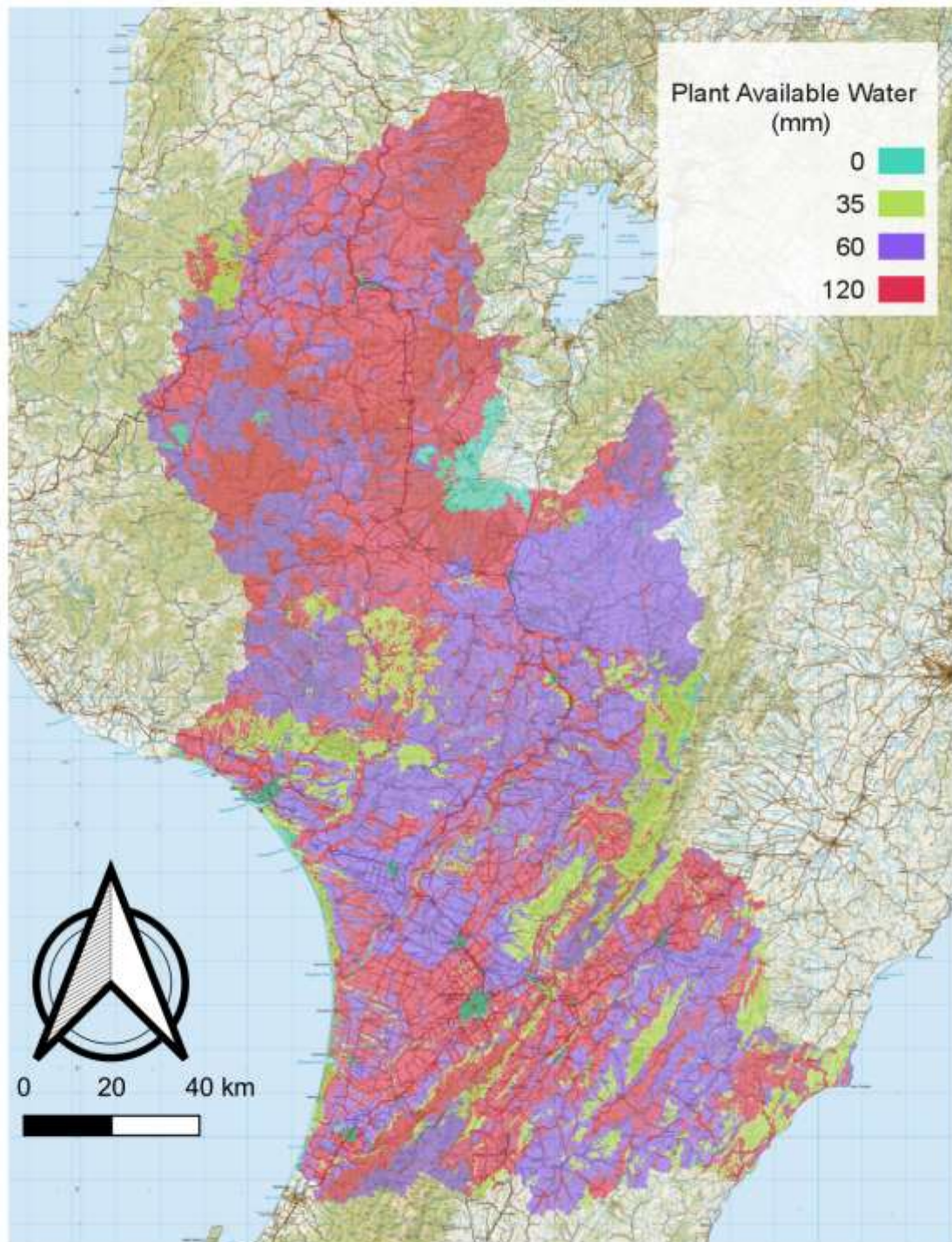
Figure 9. Soil layer representing variation in PAW in four categories.

Irrigable land was described by Bright *et al.* (2018) based on combining LUC and land slope (Figure 10).
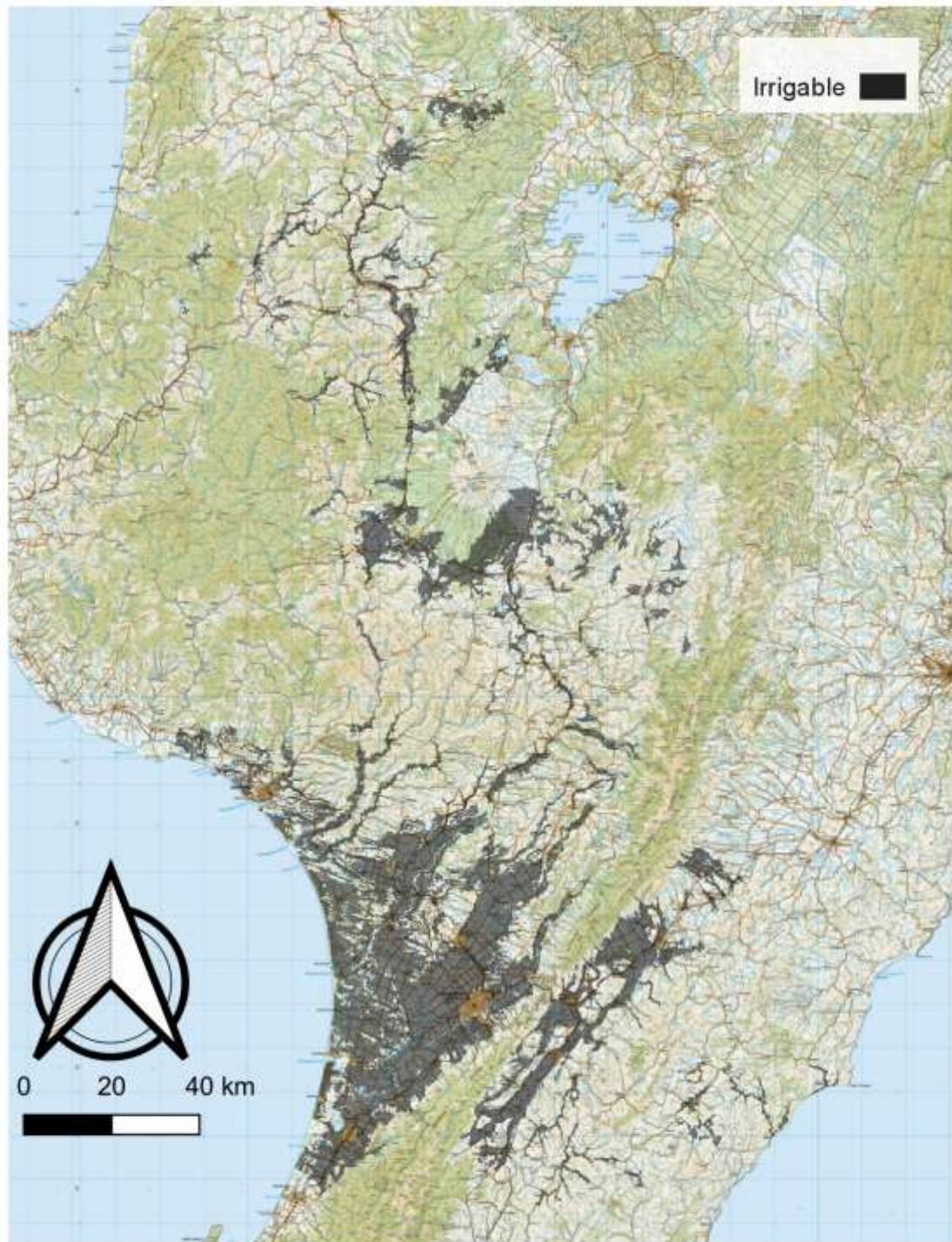
Figure 10.   Irrigable land layer representing areas that are feasibly irrigated.

Irrigated land was obtained from https://data.mfe.govt.nz/layer/90838-irrigated-land-area-2017/ (Figure 11). This layer pertains to 2017 however, there has not been a significant increase in irrigation since 2012 and it was therefore considered to be sufficiently representative (Figure 11).
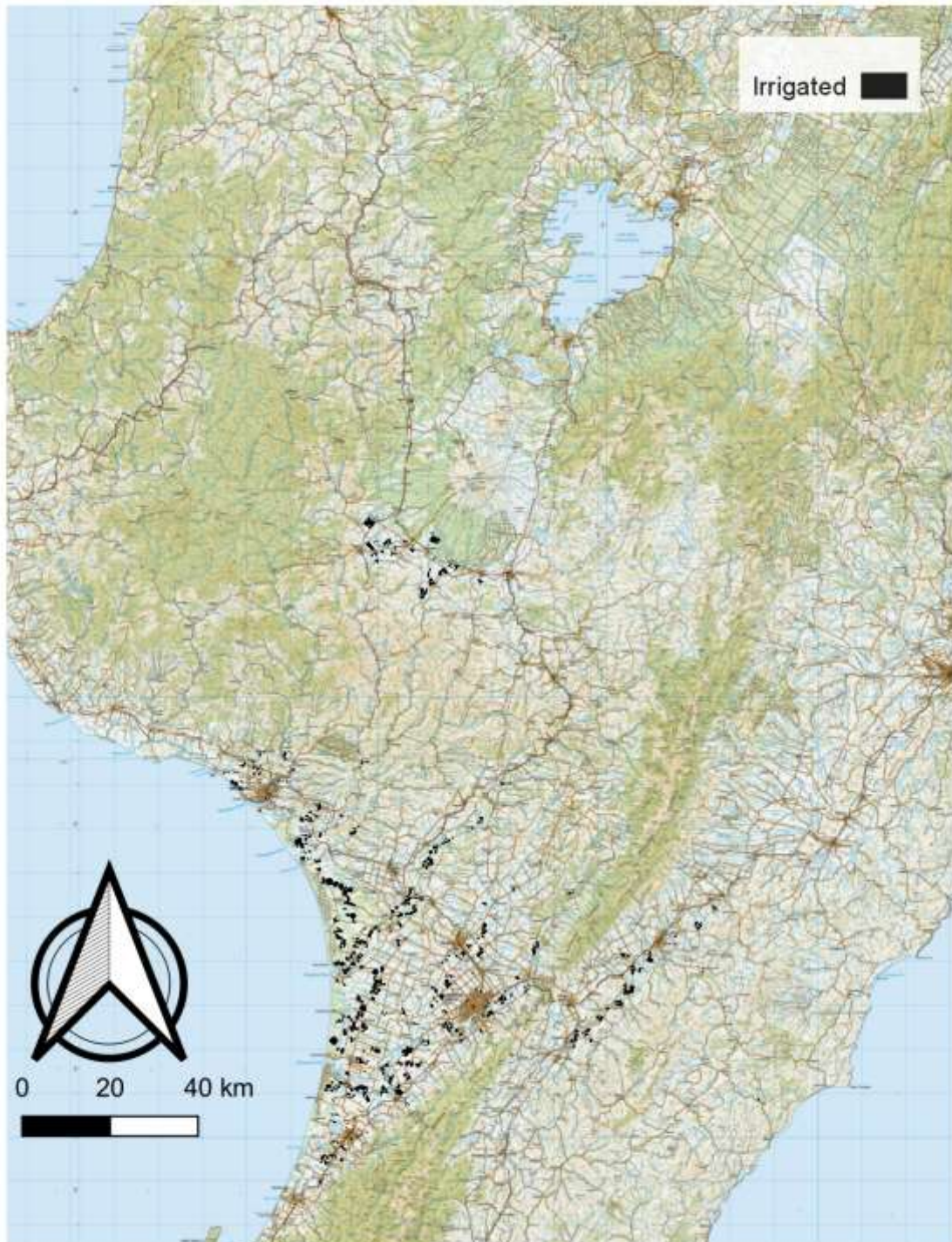
Figure 11. Irrigated land layer representing areas that are assessed to be irrigated.

Bright *et al.* (2018) provide tables of export coefficients for most combinations of the nine land use types and the categories for each of the four other biophysical factors (climate, PAW, irrigable and irrigated) that occur in the Manawatū-Whanganui Region. We made some adjustments to these export coefficients to provide a complete coverage and to incorporate regionally specific information. First, we used export coefficients from vegetable growing areas in Horowhenua based on loss rates estimated by Bloomer *et al.* (2020). Second, we increased export coefficients for non-productive land from the value of 1 kg N yr^{-1} provided by Bright *et al.* (2018) to 2 kg N yr^{-1}, which is consistent with values used by Collins *et al.* (2017) and other regional analyses. Third, we assumed export coefficients for exotic cover were 3 kg N yr^{-1} based on values used by Collins *et al.* (2017). Finally, there were areas that were classified as non-irrigable, but which were nevertheless irrigated according to the available data. We assumed that export coefficients for irrigated but non-irrigable land were the same as irrigated and irrigable land.

To assign export coefficients to all land in the region, we first subdivided each WMZ into a discrete number of grid cells based on a 250m by 250m grid. For each grid cell, the combination of the table of export coefficients with maps describing land use (Figure 7) and the four additional biophysical factors (climate, PAW, irrigable and irrigated) resulted in the distribution of diffuse source export coefficients shown in Figure 12. For each land use category, the export coefficients account for variation in four biophysical factors including: climate zone, plant available soil water capacity (PAW), and whether the land is irrigable and irrigated.

The export coefficients used by this study are general in that they are estimates of average rates, within each combination of land use and factor categories, New Zealand wide (Bright *et al.*, 2018). However, Bright *et al.*'s (2018) export coefficients systematically account for variation in nitrogen loss rates due to different types biophysical conditions (i.e., variation in the four biophysical factors). All estimates of export coefficients are subject to uncertainty and will be imprecise when compared to a specific farm property or a more exactly defined biophysical context. To provide for a degree of validation of the adopted export coefficients, we compared them with the available regionally specific estimates made by other studies. The details of these comparisons are described in Appendix C of this report. These comparisons show that there is a reasonably high level of consistency in the average values for the nitrogen export coefficients provided by the various studies (including the export coefficients that were adopted by this study) but that there is also considerable range in these values. These and other uncertainties are compounded in the models and mean our confidence is highest when the model is used to asesses the difference in water quality outcomes between two scenarios in relative terms. A formal analysis of the model uncertainty and assessment of possible differences due to land use changes is possible with the CASM models but was beyond the scope of this study.
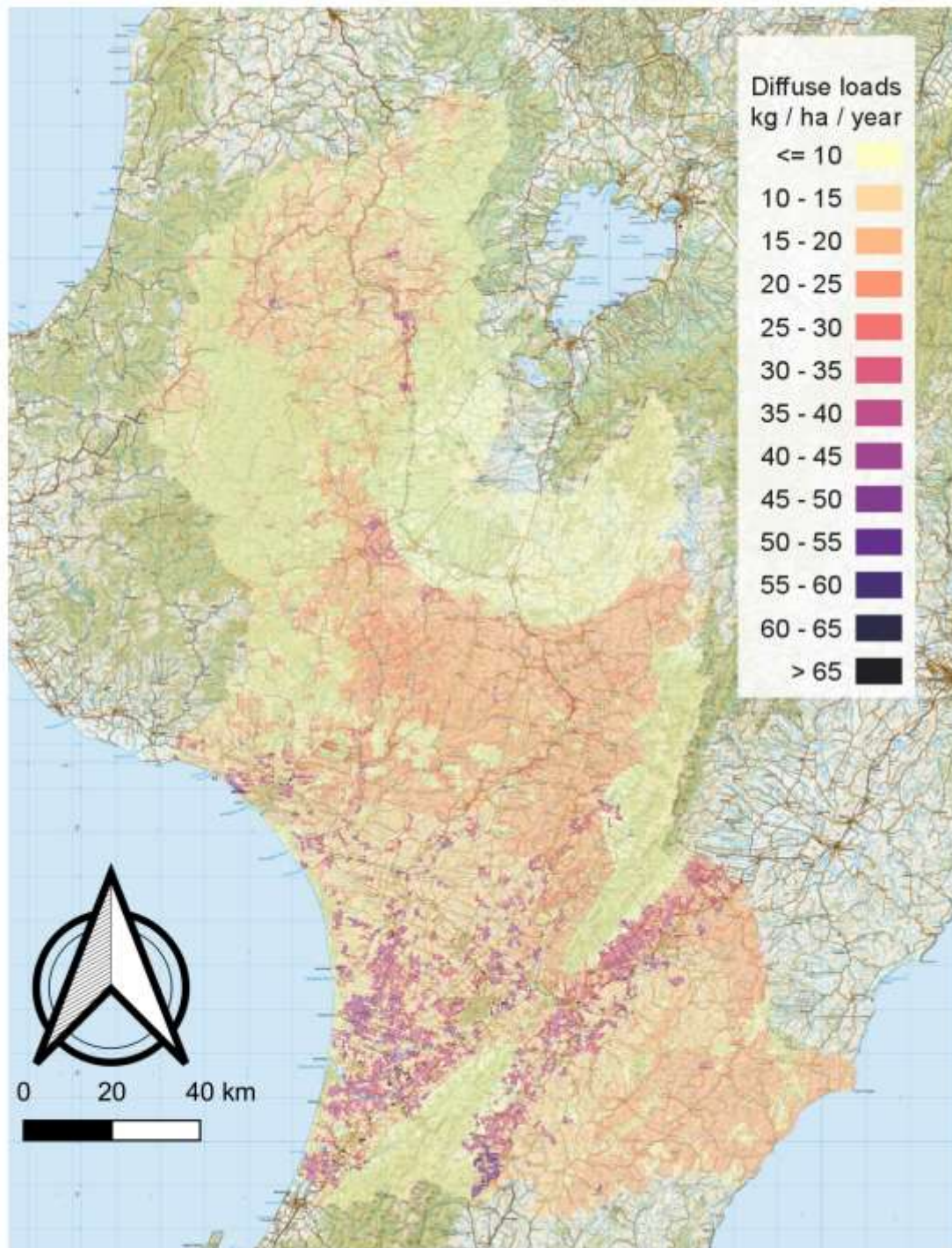
Figure 12. Variation of diffuse source export coefficients across the region. Export coefficients were derived by combining the 2012 land use map and modifications of export coefficients provided by Bright et al. (2018).

2.6   Model sub-catchment load aggregation

The land use capability (LUC) system is a national land classification framework that was developed in 1952 and has been refined since then to define biophysical constraints that may limit sustained productivity within farm management units (Lynn *et al.*, 2009; Mueller *et al.*, 2010). Table 14.2 of the One Plan allocates nitrogen loss rate limits to land based on LUC categories (categories from 1 to 8) (Figure 13). It was therefore necessary to represent LUC categories in the models so that analyses such as future scenario simulations could be defined based on LUC categories. Analyses also depend on assumptions about the land use category. Therefore, within each of the model sub-catchments (i.e., the WMZs shown in Figure 1 to Figure 4), each grid cell was assigned to the combination of its spatially dominant LUC and land use categories. Cells pertaining to each of these combined categories were aggregated within each sub-catchment and were represented in the models as separate "diffuse-source nodes". Each diffuse-source model node was parameterised with a representative export coefficient (derived from Figure 12) and total land area.
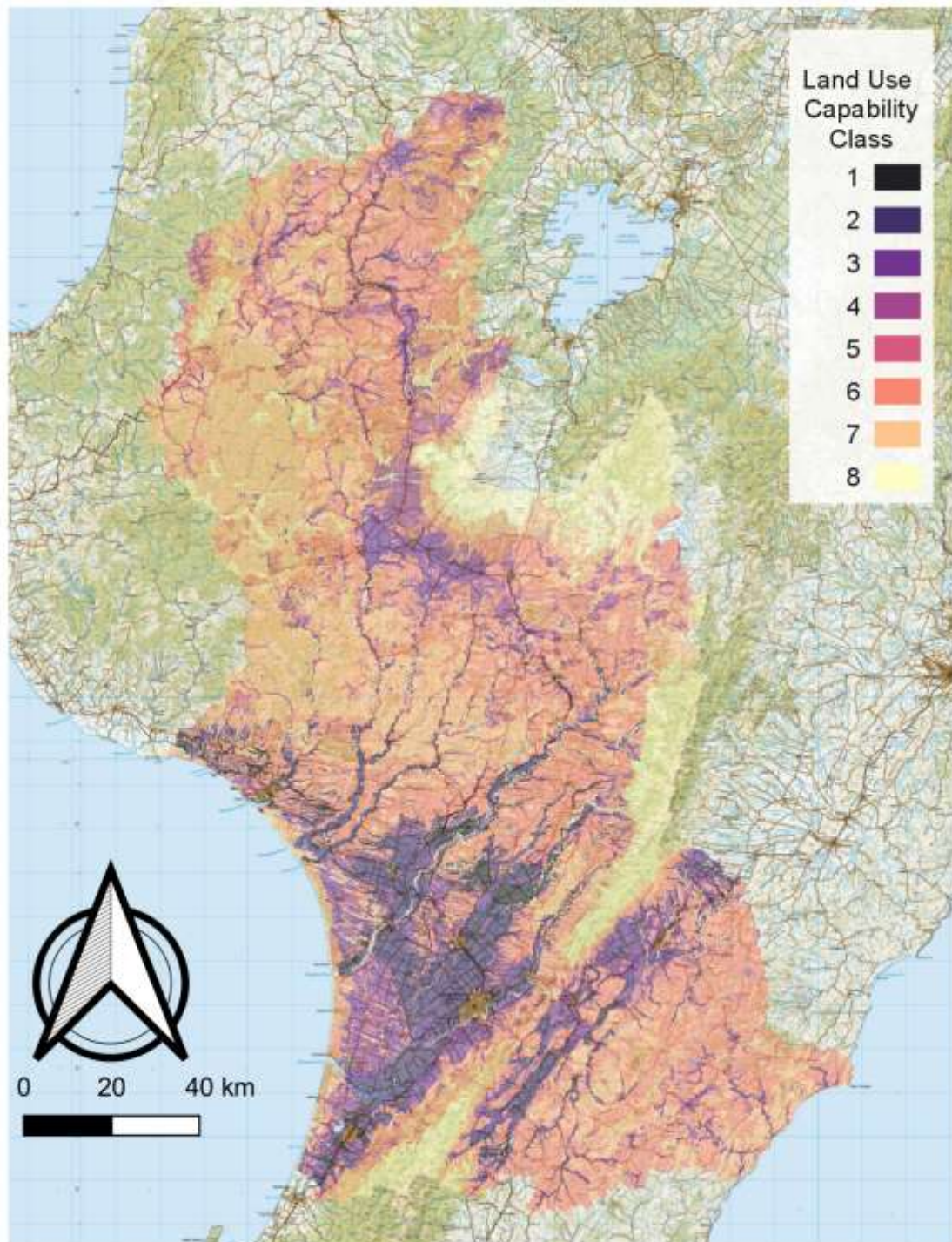
Figure 13. Land use capability (LUC) layer representing eight land use capability categories.

2.7 Model calibration

Each model was calibrated so that modelled downstream nitrogen loads and concentrations adequately matched measured data for a series of river monitoring stations. The primary calibration parameters were diffuse pathway attenuation coefficients, specific to each WMZ. Calibration proceeded from upstream to downstream with manual adjustments to upstream

attenuation coefficients, for each calibration point, to achieve an acceptable agreement in the water quality calibration targets. The calibration points, with total nitrogen (TN) concentration performance measures, are shown in Figures 5 – 8 and summarised in Tables 3 - 6. In a small number of cases, export coefficients also required adjustment to achieve an acceptable calibration.

Note that, for some water quality stations, river kilometre marker locations were adjusted slightly to be downstream of contributing WMZs. In such cases, we expect modelled concentrations to be slightly higher than measured (because the model has effectively artificially added additional diffuse load). In other cases, the water quality station includes drainage area not included in the upstream WMZ discretization. In these cases, we expect modelled concentrations to be lower than measured. These sites are indicated in the summary tables.

The calibration process generally followed the steps listed below.

1. The calibration was performed for each water quality station calibration point in sequence, moving from upstream to downstream.

2. For each calibration point, all upstream uncalibrated diffuse node attenuation coefficients were uniformly adjusted to achieve acceptable modelled vs. measured TN concentrations. For all nodes, the model default minimum attenuation of 0.1 was maintained.

3. If an acceptable calibration couldn't be achieved with adjustments to attenuation coefficients alone, sensible adjustments were made to node export coefficients. For this study, this step only ever involved an increase in export coefficients from original independent parameterisation. For example, for some WMZs the minimum export coefficient was increased from 1 to 2 kg ha^{-1} yr^{-1} to 4 kg ha^{-1} yr^{-1} (e.g. for native and exotic cover).

4. Calibration performance was assessed based on professional judgement, but in most cases modelled results were within 10 – 20% of measured values.

5. For unmonitored WMZs, without a corresponding downstream calibration point, attenuation coefficients were assigned based on nearest neighbour calibrated values.

3 Results

3.1 Calibration of attenuation

Summaries of calibrated diffuse attenuation coefficients are provided in Table 2 to Table 5 and on Figure 14 to Figure 17. A satisfactory calibration was achieved for all four basin models. Downstream calibration targets were all achieved with sensible adjustments to upstream attenuation coefficients, within expected ranges, and, in a limited number of cases, minor adjustments to independently derived export coefficients. In general, a pleasing consistency in calibrated attenuation coefficients was achieved within a given basin model. For example, a uniform attenuation coefficient of 0.1 (model minimum) was calibrated for the entirety of the Whanganui basin. For the Whangaehu basin, greater than 90% of catchment attenuation, by area, was calibrated within the range of 0.35 to 0.65. A general gradient of high to low attenuation from upland to lowland sub-catchments was apparent in both the Manawatū and Rangitikei basins (Figure 18). Variability in attenuation coefficients throughout the region is driven by a range of potential factors, including sub-catchment size,

land cover, hydrology, and physiography. Further investigation into this variability is beyond the scope of the current study.

Table 2. Manawatū River basin model calibration results: annual average TN concentrations and load.

Water Quality Station	Modelled, (mg/L)	Measured (mg/L)	Unattenuated (t/y)	Attenuated (t/y)
Manawatū at Weber Road	1.6	1.6	1196	652
Manawatū at Hopelands	1.6	1.6	2250	1421
Manawatū at Upper Gorge	1.3	1.2	5103	3305
Manawatū at Teachers College	1.2	1.3	5955	3812
Manawatū at u/s PNCC STP	1.1	1.21	5981	3491
Manawatū at ds Fonterra Longburn	1.1	1.0	6888	3881
Manawatū at Opiki Br	1.2	1.21	6999	3908
Mangatoro at Mangahei Road	1.5	1.4	341	181
Tamaki at Stephensons	1.2	1.3	108	97
Kumeti at Te Rehunga	1.2	1.5	18	16
Oruakeretaki at d/s PPCS Oringi STP	2.0	2.1	107	96
Raparapawai at Jackson Rd	1.4	1.4	87	36
Makakahi at Hamua	1.6	1.32	385	289
Mangatainoka at Larsons Road	0.4	0.4	40	36
Mangatainoka at Brewery - S.H.2 Bridge	1.6	1.6	846	677
Makuri at Tuscan Hills	1.7	1.7	225	157
Tiraumea at Ngaturi	1.3	1.3	1057	574
Mangahao at Ballance	0.4	0.4	214	193
Mangapapa at Troup Rd	1.6	1.6	45	26
Pohangina at Mais Reach	0.4	0.3	484	174
Oroua at Almadale Slackline	0.8	0.7	464	164
Oroua at d/s AFFCO Feilding	1.0	1.0	978	365
Oroua at d/s Feilding STP	1.8	1.9	1273	647
Oroua at Awahuri Bridge	1.2	1.2	1495	483
Owahanga at Branscombe Bridge	1.4	1.3	617	247
Ohau at Gladstone Reserve	0.3	0.3	56	50

Table 3. Rangitikei Model River basin model calibration results: annual average TN concentrations and load.

Water Quality Station	Modelled (mg/L)	Measured (mg/L)	Unattenuated (t/y)	Attenuated (t/y)
Rangitikei at Pukeokahu	0.21	0.21	635	159
Rangitikei at Mangaweka	0.38	0.37	2493	795
Rangitikei at Onepuhi	0.51	0.54	3442	1270
Rangitikei at Kakariki	0.49	0.48	3382	1264
Rangitikei at McKelvies	0.84	0.87	4517	2320
Hautapu at Alabasters	0.68	0.68	313	94

Table 4. Whanganui River basin model calibration results: annual average TN concentrations and load.

Water Quality Station	Modelled (mg/L)	Measured (mg/L)	Unattenuated (t/y)	Attenuated (t/y)
Whanganui at Te Maire	0.59	0.58	1641	1478
Whanganui at Pipiriki	0.68	0.67	4903	4415
Whanganui at Te Rewa	0.67	0.72	5350	4816
Whanganui at Paetawa	0.67	0.70	5350	4816
Ongarue at Taringamotu	0.75	0.76	949	854
Ohura at Tokorima	1.1	1.1	902	812

Table 5. Whangaehu River basin model calibration results: annual average TN concentrations and load.

Water Quality Station	Modelled (mg/L)	Measured (mg/L)	Unattenuated (t/y)	Attenuated (t/y)
Whangaehu at Kauangaroa	0.84	0.84	2390	1194
Tokiahuru at Junction	0.19	0.19	54	49
Makotuku at d/s Raetihi STP	0.71	0.60	129	54
Mangawhero at Pakihi Rd Bridge	0.55	0.52	154	89
Mangawhero at Raupiu Road	0.82	0.82	986	459
Turakina at ONeills Bridge	3.6	3.5	1586	951
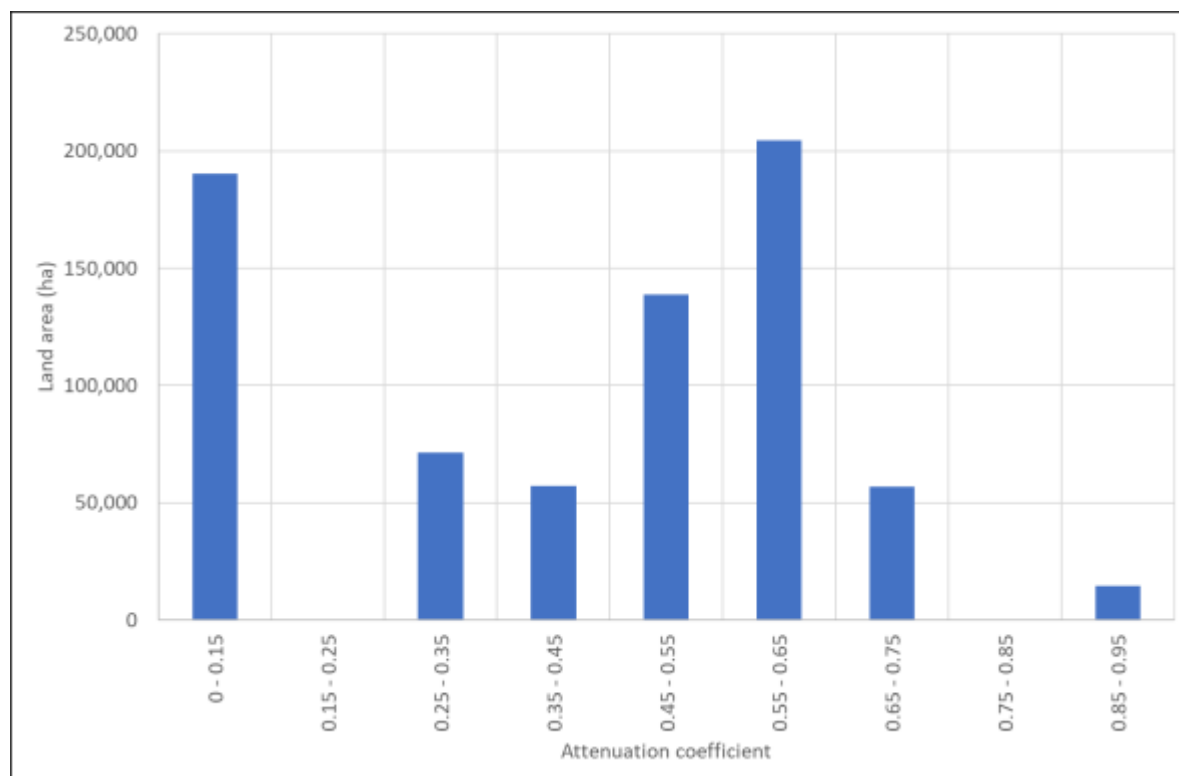
Figure 14. Areal distribution of calibrated attenuation coefficients, Manawatū River basin
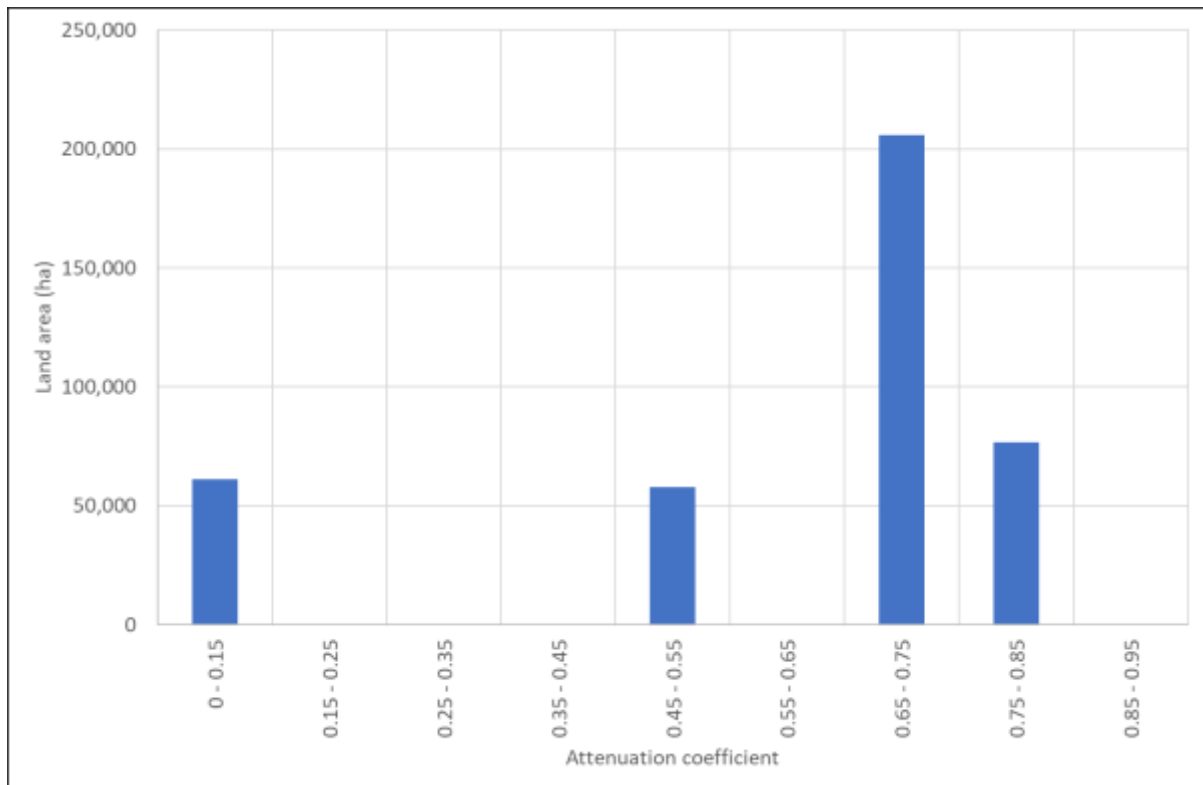
Figure 15. Areal distribution of calibrated attenuation coefficients, Rangitīkei River basin
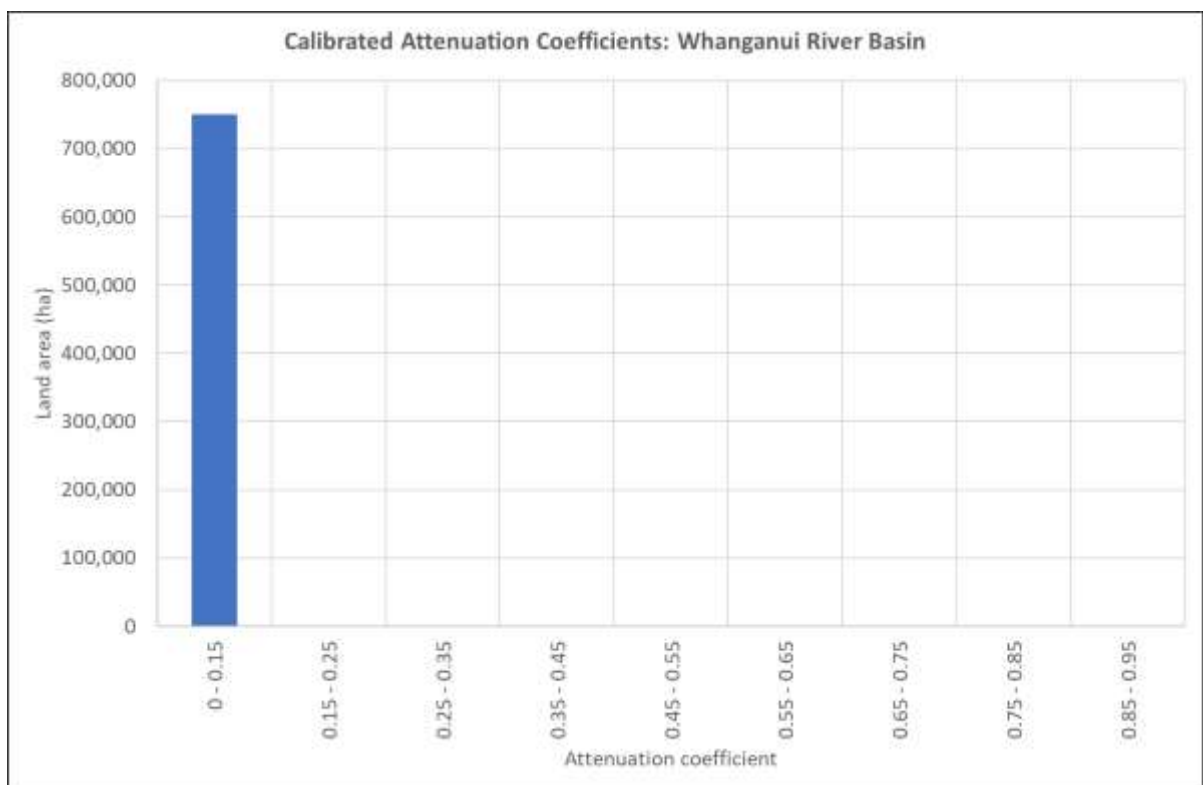
Figure 16. Areal distribution of calibrated attenuation coefficients, Whanganui River basin
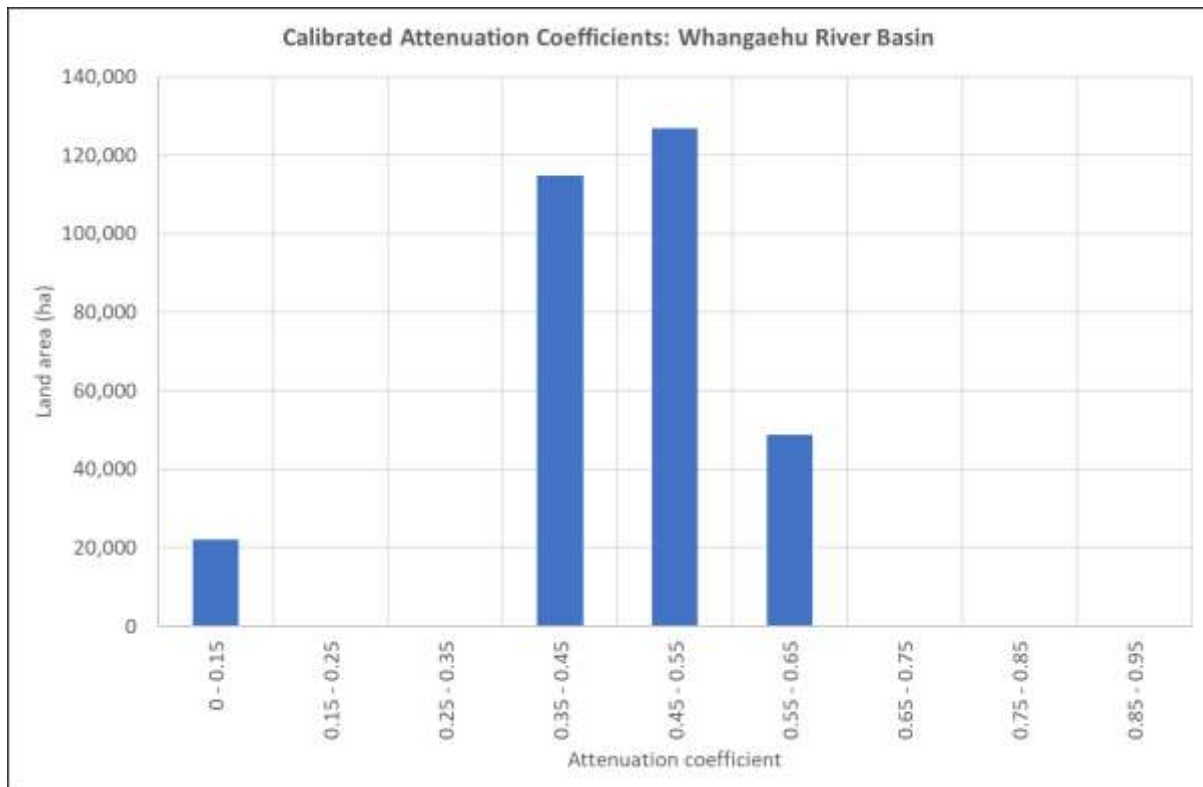
Figure 17. Areal distribution of calibrated attenuation coefficients, Whangaehu River basin
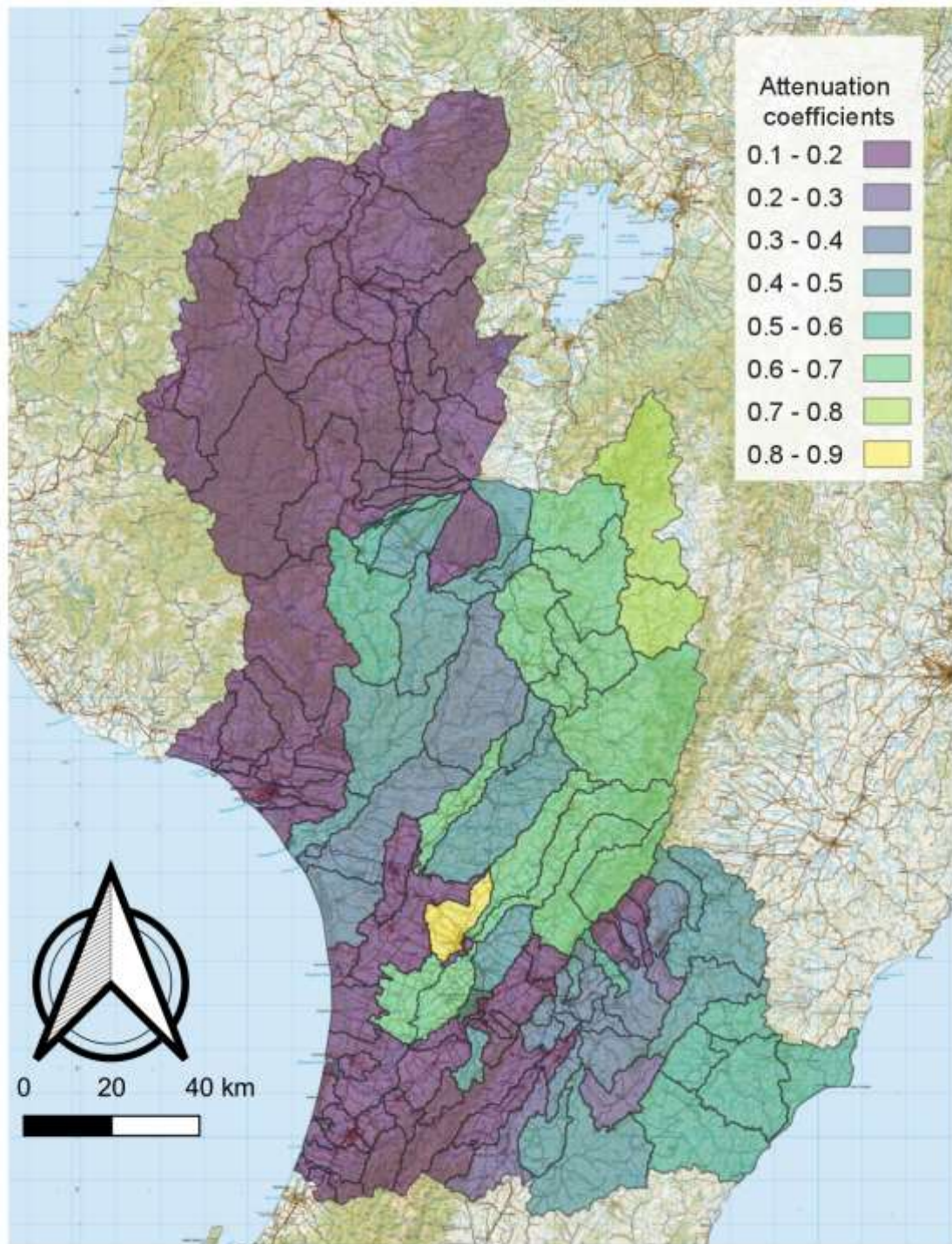
Figure 18. Map showing attenuation rates for each WMZ represented in the models.

3.2 Comparison with previous load calculations and uncertainties associated with attenuation estimates

Singh & Elwan (2017) calculated TN loads at 34 water quality stations that were common to this study. Singh & Elwan (2017) used the flow stratification method (see Appendix A) and concentration and flow data pertaining to the period from January 2012 to December 2016. We compared the water quality station loads estimated by Singh & Elwan (2017) with the loads estimated by this study.

This study's load estimates are systematically higher than those of Singh and Elwan (2017) (Figure 19). There are two potential explanations for these differences. First, even with identical input data, different load calculation methods produce different results and these differences can be systematic (i.e., leading to a consistent difference; Defew *et al.*, 2013; Roygard *et al.*, 2012). Second, loads estimated at the same site, but for different time periods can vary significantly (Snelder *et al.*, 2017). The loads estimated by the current study pertained to a specific year (2012), which was possible because the calculation methods involved a temporal term (see Appendix A). The flow stratification method used by Singh and Elwan (2017) does not involve a temporal term and therefore the load estimate can be considered to represent the mean annual load for the entire period of record used in the calculation.

Figure 19. Comparison of load estimates for 34 water quality stations made by this study and Singh and Elwan (2017).The error bars indicate the 95% confidence interval for the load estimates made by this study. The red (1 to 1) line indicates perfect correspondence between the two estimates. Note that the axes are log scales.

We examined whether the systematic differences in loads estimated by the two studies could be associated with differences in the time-periods implied by the calculation methods. We examined trends in TN concentrations at the 34 water quality stations over the period used to calculate the loads by Singh and Elwan (2017). Raw (i.e., not flow adjusted) trends for these sites were produced by Fraser and Snelder (2018) for the five year period ending in 2017 (i.e. 2013 to 2017 inclusive), which closely corresponds to the period from January 2012 to December 2016 period used by Singh and Elwan (2017). We summarised the TN trends in two ways. First, we used the proportion of improving trends (PIT; Fraser and Snelder, 2018) to represent the overall trend direction over the 34 sites. The PIT statistic had a value of 82% (standard error = ±5%), which indicates 82% of sites had improving (i.e., decreasing) TN trends in the period. Second, each of the 34 trends was assigned to a category indicating confidence that the trend was improving. The summary of the proportions of sites in each category indicates that ~75% of sites were at least likely to have improved over the period (Figure 19). Only ~9% of sites were unlikely (or less probable) to have had improving trends (i.e., the equivalent of the complementary probability they were at least likely to have degraded). The decreasing TN trends over most sites in the period between 2013 to 2017 is broadly consistent with the systematically higher load estimates made by this study. This study's higher estimates pertain to the start of the period (2012) whereas the estimates made by Singh and Elwan (2017) pertain to average over the period in which concentrations decreased at most sites.
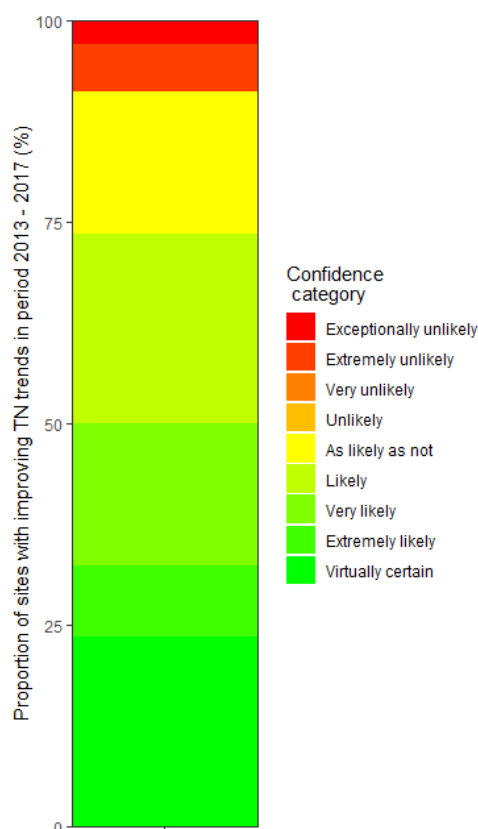
Figure 20. Summary plot representing the proportion of the 34 sites with improving 5-year time period trends at each categorical level of confidence. The plot shows the proportion of sites for which water quality was improving at nine levels of confidence defined by (Fraser and Snelder, 2018). Green colours indicate improving sites, and red-orange colours indicate degrading sites. Trends used in this graph are not flow adjusted.

Other studies have estimated nitrogen attenuation factors (AF_N) for the same water quality stations represented by this study (e.g., Elwan *et al.*, 2015). We calculated effective net attenuation coefficients, AF_N, for the 34 water quality stations in common to this study and Singh and Elwan (2017). These net attenuation coefficients represent the combined result of all upstream diffuse-source node calibrated attenuation coefficients, combined with upstream unattenuated point sources, and were calculated as follows:

$$AF_N = \frac{L_c - L_{wqs}}{L_c}$$

<div align="right">*Equation 1*</div>

where L_c is the estimated catchment source load (including the diffuse and point sources) and L_{wqs} is the estimated water quality station load. These values have the same physical meaning as the attenuation coefficients derived by the CASM calibration. However, in the discussion that follows we refer to them as AF_N values because we are not referring directly to the CASM attenuation coefficients.

Close agreement between AF_N values estimated by different studies is unlikely due to two sources of uncertainty. First, as described above, estimates of loads for the same water quality station are likely to vary between load calculation methods and time periods. Second, to estimate attenuation, an estimate of the catchment source loads is required, and this calculation is likely to differ considerably between studies and to be uncertain.

We demonstrate the range of uncertainty of AF_N estimates made using the data provided by this study. We compare this study's AF_N values with those estimated using the same catchment source loads but with the 34 water quality station loads estimated by Singh and Elwan (2017) that are in common. We estimated the uncertainty of this study's AF_N values by combining the uncertainty of the water quality station load estimates with an assumed uncertainty of the catchment source loads using the following relationship:

$$\frac{u(AF_N)}{AF_N} = \sqrt{\left[\frac{u(L_{wqs})}{L_{wqs}}\right]^2 + \left[\frac{u(L_c)}{L_c}\right]^2}$$

<div align="right">*Equation 2*</div>

where, $u(AF_n)/AF_N$ is the relative uncertainty in the estimate of the nitrogen attenuation factor, $u(L_{wqs})/L_{wqs}$ is the relative uncertainty in the estimated water quality station load and, $u(L_c)/L_c$ is the relative uncertainty in the estimated catchment source load. We assumed a relative uncertainty of the estimated catchment source load of 25%, which was based on an estimated characteristic uncertainty for the OVERSEER nutrient budgeting model (PCE, 2018).

Large uncertainty in the estimates of AF_N for most sites is shown in Figure 21. Figure 21 also indicates that AF_N estimated using water quality station loads estimated by Singh and Elwan (2017) are systematically lower (by about 0.2) compared to the estimates made using water quality station loads estimated by this study. The reason for this difference is the systematic difference in site loads between the two studies that is shown in Figure 19. Higher water quality station loads estimated by this study leads to lower AF_N estimates compared to estimates using the loads of Singh and Elwan (2017). However, the 95% confidence intervals indicate that for individual sites, the uncertainty in AF_N estimated by this study always encompass the value of AF_N if the water quality station loads estimated by Singh and Elwan (2017) were used. In other words, the published Singh and Elwan (2017) values fall within the estimated confidence intervals for this study.
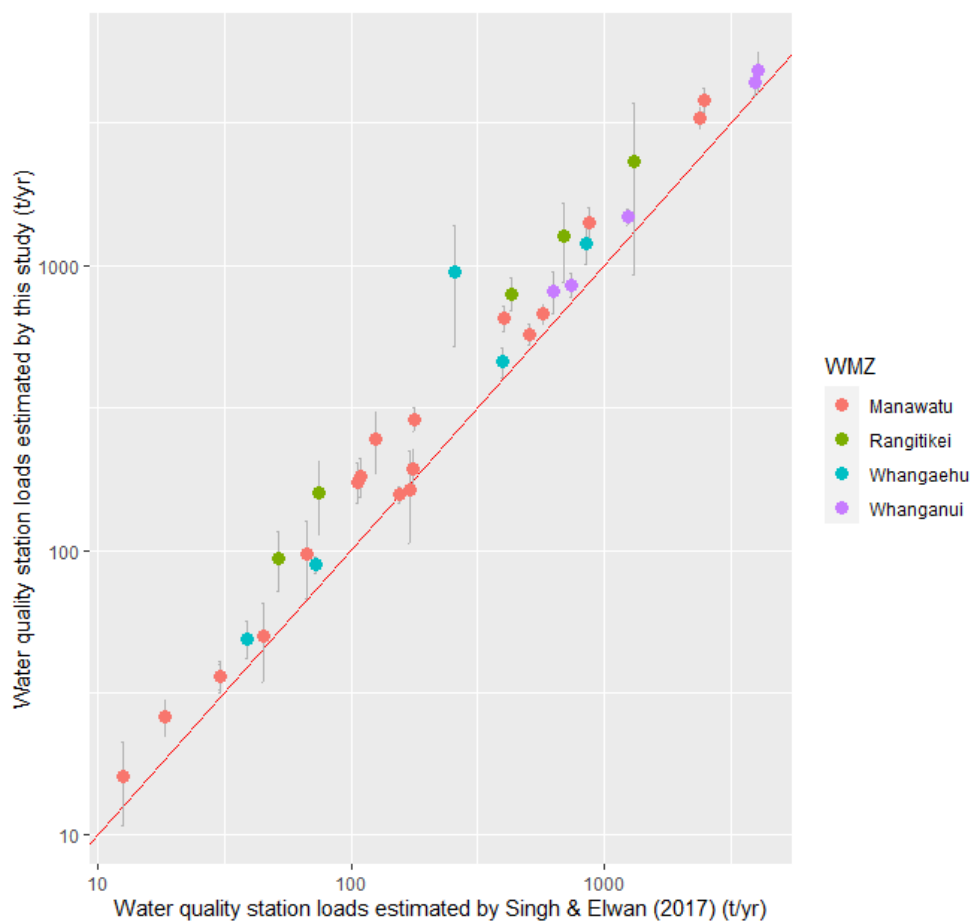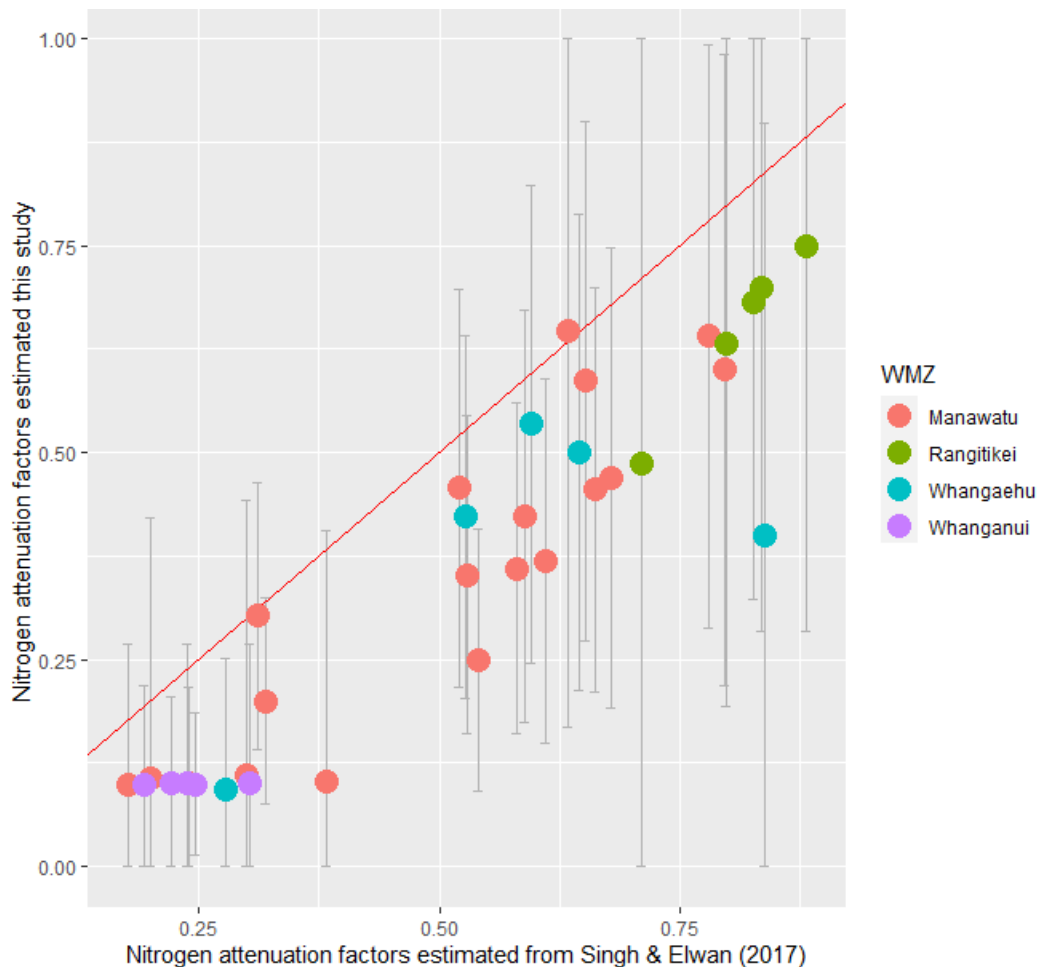
Figure 21. Comparison of AF_N estimated using load estimates for 34 water quality stations made by this study and (Singh and Elwan, 2017).The error bars indicate the 95% confidence intervals for AF_N estimates for this study.

4   Conclusion

Catchment water quality models were developed for the four major river basins in the Horizons Region: the Manawatū (including the Horowhenua and Coastal Tararua catchments), the Rangitikei, the Whanganui, and the Whangaehu (including the Turakina River catchment). The entire region is encapsulated by the four models. The models use sub-catchment export and attenuation coefficients to simulate the generation, transport, and downstream delivery of total nitrogen loads throughout the region. The models were developed to investigate the impact of regulating nitrogen discharge allowances from intensively farmed land throughout the region, particularly with respect to mitigation implications and feasibility. The models were developed in a usable framework to allow for future application by a range of potential end users.

A satisfactory calibration was achieved for all four basin models. Downstream calibration targets were all achieved with sensible adjustments to upstream attenuation coefficients, within expected ranges, and, in a limited number of cases, minor adjustments to independently derived export coefficients. Patterns of attenuation within, and between, basins have been noted but not yet fully explained.

Ideally, water quality models are calibrated to land use and catchment nitrogen emission estimates that are congruent and pertain to a specific point in time. In this study, the available land use map and catchment nitrogen emission data were not congruent in time. Limitations associated with data meant that models were calibrated to the land use pattern pertaining to 2008 and to diffuse source export coefficients and water quality station loads pertaining to 2012. However, we consider these inconsistencies are acceptable due to the relatively imprecise nature of the nitrogen emission estimates. Taken together, the uncertainties in the model input data mean that potential differences in model predictions resulting from the non-congruence of dates for the land use and catchment nitrogen emission estimates and the baseline are unlikely to be statistically significant (i.e., any differences would be within the model uncertainty). A formal analysis of the model uncertainty and assessment of possible differences due to land use changes is possible with the CASM models but was beyond the scope of this study.

Models are uncertain, and the uncertainty of the key model parameter (attenuation coefficient) has been demonstrated in this report. This uncertainty is largely unavoidable and results from uncertainty in the water quality station loads and estimated sub-catchment source loads. This uncertainty needs to be considered when using the models to make simulations of future scenarios. The absolute values of load and concentrations predicted for a scenario should be regarded as less certain than the relative change. Like most models, these catchment models are better suited for predicting relative changes in basin water quality rather than absolute values. In other words, it may be wise to frame future scenario simulation results in terms of relative changes compared to the "baseline" models presented here. Further, applying relative (e.g. percentage) changes to model input parameters (e.g. export coefficients) may be a more defensible approach for scenario simulations than prescribing absolute values. That said, these models represent the best available science for investigating the fundamental questions of the wider study and can serve as valuable supporting tools for decision-making.

Acknowledgements

References

Bloomer, D., G. O'Brien, and L. Posthuma, 2020. Modelled Loss of Nutrients From Vegetable Growing Scenarios In Horowhenua. Page Bloomer Associates, New Zealand.

Bright, J., S. Ford, and C. Irving, 2018. Water Allocation Economics Analysis: Land/Water Use Modelling. Aqualinc client report, Aqualinc Research Limited, Christchurch, New Zealand.

Cohn, T.A., 2005. Estimating Contaminant Loads in Rivers: An Application of Adjusted Maximum Likelihood to Type 1 Censored Data. Water Resources Research 41. http://onlinelibrary.wiley.com/doi/10.1029/2004WR003833/full. Accessed 21 Jan 2016.

Cohn, T.A., D.L. Caulder, E.J. Gilroy, L.D. Zynjuk, and R.M. Summers, 1992. The Validity of a Simple Statistical Model for Estimating Fluvial Constituent Loads: An Empirical Study Involving Nutrient Loads Entering Chesapeake Bay. Water Resources Research 28:2353–2363.

Cohn, T.A., L.L. Delong, E.J. Gilroy, R.M. Hirsch, and D.K. Wells, 1989. Estimating Constituent Loads. Water Resources Research 25:937–942.

Collins, S., R. Singh, A. Rivas, A. Palmer, D. Horne, A. Manderson, J. Roygard, and A. Matthews, 2017. Transport and Potential Attenuation of Nitrogen in Shallow Groundwaters in the Lower Rangitikei Catchment, New Zealand. Journal of Contaminant Hydrology 206:55–66.

Defew, L.H., L. May, and K.V. Heal, 2013. Uncertainties in Estimated Phosphorus Loads as a Function of Different Sampling Frequencies and Common Calculation Methods. Marine and Freshwater Research 64:373–386.

Duan, N., 1983. Smearing Estimate: A Nonparametric Retransformation Method. Journal of the American Statistical Association 78:605–610.

Efron, B., 1981. Nonparametric Estimates of Standard Error: The Jackknife, the Bootstrap and Other Methods. Biometrika 68:589–599.

Elwan, A., R. Singh, D. Horne, J. Roygard, and B. Clothier, 2015. Nitrogen Attenuation Factor: Can It Tell a Story about the Journey of Nutrients in Different Subsurface Environments. Proc Moving Farm Systems to Improved Attenuation. Fertiliser and Lime Research Centre, Massey University.

Fraser, C. and T. Snelder, 2018. State and Trends of River Water Quality in the Manawatū-Whanganui Region. LWP Ltd, Christchurch, New Zealand.

Fraser, C.E. and T. Snelder, 2019. Test of Methods for Calculating Contaminant Loads in the Manawatū-Whanganui Region: Supplementary Report. LWP Ltd, Christchurch.

Fraser, C. and T. Snelder, 2020. Load Calculations and Spatial Modelling of State, Trends and Contaminant Yields. For the Manawatū-Whanganui Region to December 2017. Client Report, LWP Ltd, Christchurch, New Zealand.

Lynn, I.H., A.K. Manderson, M.J. Page, G.R. Harmsworth, G.O. Eyles, G.B. Douglas, A.D. Mackay, and P.J.F. Newsome, 2009. Land Use Capability Survey Handbook. A New Zealand Handbook for the Classification of Land. AgResearch, Landcare Research, GNS Science, Hamilton, Lincoln, Lower Hutt, New Zealand.

Manderson, A., 2015. Nitrogen Leaching Estimates for Sheep and Beef Farming in the Mangatainoka Catchment. Horizons Regional Council, Palmerston North, New Zealand.

Manderson, A., L. Lilburne, and V. Vetrova, 2016. Spatial OVERSEER N-Loss Modelling for the Rangitikei Catchment. Landcare Research Client report, Palmerston North, New Zealand.

Mueller, L., U. Schindler, W. Mirschel, T.G. Shepherd, B.C. Ball, K. Helming, J. Rogasik, F. Eulenstein, and H. Wiggering, 2010. Assessing the Productivity Function of Soils. A Review. Agronomy for Sustainable Development 30:601–614.

Parker, W.J., 1998. Standardisation between Livestock Classes: The Use and Misuse of the Stock Unit System. Proceedings of the Conference New Zealand Grassland Association., pp. 243–248.

PCE, 2018. Overseer and Regulatory Oversight: Models, Uncertainty and Cleaning up Our Waterways. Parliamentary Commissioner for the Environment, Wellington, New Zealand. https://www.pce.parliament.nz/media/196493/overseer-and-regulatory-oversight-final-report-web.pdf.

Roygard, J.K.F., K.J. McArthur, and M.E. Clark, 2012. Diffuse Contributions Dominate over Point Sources of Soluble Nutrients in Two Sub-Catchments of the Manawatu River, New Zealand. New Zealand Journal of Marine and Freshwater Research 46:219–241.

Singh, R. and A. Elwan, 2017. Resource Accounting in the Manawatu-Wanganui Region. Science report, Horizons Regional Council, Palmerston North, New Zealand.

Singh, R., A. Elwan, and D. Horne, 2017. Nitrogen Accounting in the Rangitikei Catchment. Horizons Regional Council Report, Horizons Regional Council, Palmerston North, New Zealand.

Snelder, T.H., R.W. McDowell, and C.E. Fraser, 2017. Estimation of Catchment Nutrient Loads in New Zealand Using Monthly Water Quality Monitoring Data. JAWRA Journal of the American Water Resources Association 53:158–178.

Appendix A   Water quality station load calculations

A1   General approach

Mean annual TN loads at all water quality stations in 2012 were derived from monthly TN concentrations and observed or modelled daily flows. Load calculation methods generally comprise two steps: (1) the generation of a series of flow and concentration pairs representing 'unit loads' and (2) the summation of the unit loads over time to obtain the total load. In practice step 1 precedes step two but in the explanation that follows, we describe step 2 first.

If flow and concentration observations were available for each day, the export coefficient, (the mean annual load, standardised by the upstream catchment area) would be the summation of the daily flows multiplied by their corresponding concentrations:

$$L = \frac{K}{A_c N} \sum_{j=1}^{N} C_j Q_j \qquad\qquad \textit{(Equation 3)}$$

where L: mean annual export coefficient (kg yr^{-1} ha^{-1}), A_c: catchment area, ha, K: units conversion factor (31.6 kg s mg^{-1} yr^{-1}), C_j: TN concentration for each day in period of record (mg m^{-3}), Q_j: daily mean flow for each day in period of record (m^3 s^{-1}), and N: number of days in period of record.

In this summation, the individual products represent unit loads. Because concentration data are generally only available for infrequent days (i.e., generally in this study, monthly observations), unit loads can only be calculated for these days. However, flow is generally observed continuously, or the distribution of flows can be estimated for locations without continuous flow data, and there are often relationships between concentration and flow, time and/or season. Rating curves exploit these relationships by deriving a relationship between the sampled nutrient concentrations (c_i) and simultaneous observations of flow (q_i). Depending on the approach, relationships between concentration and time and season may be included in the rating curve. This rating curve is then used to generate a series of flow and concentration pairs (i.e., to represent Q_j and C_j in equation 1) for each day of the entire sampling period (i.e., step 1 of the calculation method; Cohn *et al.*, 1989). The estimated flow and concentration pairs are then multiplied to estimate unit loads, and these are then summed and transformed by K, N and A_c to estimate mean annual export coefficients (i.e., step 2 of the calculation method; Equation 1).

There are a variety of approaches to defining rating curves. Identifying the most appropriate approach to defining the rating curve requires careful inspection of the available data for each site and contaminant. The details of the approaches and the examination of the data are summarised below. Further details are provided by Fraser and Snelder (2019).

A2   Load calculation methods

A2.1   L7 model

Two regression model approaches to defining rating curves of (Cohn *et al.*, 1989, 1992) and (Cohn, 2005) are commonly used to calculate loads. The regression models relate the log of concentration to the sum of three explanatory variables: discharge, time, and season. The L7 model is based on seven fitted parameters given by:

$$ln(\widehat{C}_i) = \beta_1 + \beta_2 \left[ln(q_i) - \overline{(ln(q))}\right] + \beta_3 \left[ln(q_i) - \overline{(ln(q))}\right]^2 + \beta_4(t_i - \overline{T})$$
$$+ \beta_5(t_i - \overline{T})^2 + \beta_6 sin(2\pi t_i) + \beta_7 cos(2\pi t_i)$$

(Equation 4)

where, i is the index for the concentration observations, $\beta_{1,2,..7}$: regression coefficients, t_i: time in decimal years, $\overline{T}$: mean value of time in decimal years, $\overline{(ln(q))}$ mean of the natural log of discharge on the sampled days, and $\widehat{C}_i$: is the estimated i^{th} concentration.

The coefficients are estimated from the sample data by linear regression, and when the resulting fitted model is significant ($p < 0.05$), it is then used to estimate the concentration on each day in the sample period, $ln(\widehat{C}_j)$. The resulting estimates of $ln(\widehat{C}_j)$ are back-transformed (by exponentiation) to concentration units. Because the models are fitted to the log transformed concentrations the back-transformed predictions were corrected for retransformation bias. We used the smearing estimate (Duan, 1983) as a correction factor (S):

$$S = \frac{1}{n}\sum_{i=1}^{n} e^{\widehat{\varepsilon}_i}$$

(Equation 5)

where, $\widehat{\varepsilon}$ are the residuals of the regression models, and n is the number of flow-concentration observations. The smearing estimate assumes that the residuals are homoscedastic and therefore the correction factor is applicable over the full range of the predictions.

The average annual load is then calculated by combining the flow and estimated concentration time series:

$$L = \frac{KS}{N} \sum_{j=1}^{N} \widehat{C}_j Q_j$$

(Equation 6)

If the fitted model is not significant, $\widehat{C}_j$ is replaced by the mean concentration and S is unity.

To provide an estimate of the load at a specific date, (in this study t^{est} = 1/12/2012) a transformation is performed so that the year components of all dates (t_j) are shifted such that all transformed dates lie within a one-year period centred on the proposed observation date (i.e. Y=1/6/2012 to 31/6/2013).

$$ln\left(\widehat{C}_j^Y\right) = \beta_1 + \beta_2 \left[ln(q_j) - \overline{(ln(q))}\right] + \beta_3 \left[ln(q_j) - \overline{(ln(q))}\right]^2 + \beta_4(Y_j - \overline{T})$$
$$+ \beta_5(Y_j - \overline{T})^2 + \beta_6 sin(2\pi Y_j) + \beta_7 cos(2\pi Y_j)$$

(Equation 7)

where $\widehat{C}_j^Y$ is the estimated j^{th} concentration for the estimation year, and Y_j is the transformed date of the ith observation, and all other variables are as per equation 6. We use this approach to estimate loads for the analysis that are representative of the middle of the stated time period (i.e. the full calendar year of 2012

). The regression coefficients ($\beta_{1,2,..7}$) are those derived from fitting Equation 7 to the observation dataset. It follows that the estimated load for the year of interest can be calculated by:

$$L^Y = \frac{KS}{N} \sum_{j=1}^{N} \widehat{C}_j^Y Q_j$$

(Equation 8)

4.1.1.1 L5 Model

The L5 model is the same as the L7 model except that two quadratic terms are eliminated:

$$ln(\widehat{C_i}) = \beta_1 + \beta_2\big(ln(q_i)\big) + \beta_3(t_i) + \beta_4 sin(2\pi t_i) + \beta_5 cos(2\pi t_i) \qquad \text{(Equation 9)}$$

The five parameters are estimated, and loads are calculated in the same manner as the L7 model. Following the approach outlined for the L7 model, the L5 model can be adjusted when used for prediction to provide estimates for a selected load estimation date:

$$ln\left(\widehat{C_j^Y}\right) = \beta_1 + \beta_2\big[ln(q_j)\big] + +\beta_4(Y_j - \overline{T}) + \beta_6 sin(2\pi Y_j) + \beta_7 cos(2\pi Y_j) \qquad \text{(Equation 10)}$$

A2.2 Flow stratification

Roygard *et al.* (2012) employed a flow stratification approach to defining rating curves. This approach is based on a non-parametric rating curve, which is defined by evaluating the mean concentration within equal increments of the flow probability distribution (flow 'bins'). In their application, Roygard *et al.* (2012) employed ten equal time-based categories (flow decile bins), defined using flow distribution statistics and then calculated mean concentrations within each bin. This non-parametric rating curve can then be used to estimate nutrient concentrations, $\hat{C}$, for all days with flow observations. At step 2, the load is calculated using Equation 11, providing an estimate of average annual load over the observation time period.

$$L = \frac{K}{N} \sum_{j=1}^{N} \hat{C}_j Q_j \qquad \textit{(Equation 11)}$$

where $\widehat{C}_j$ is calculated mean concentration associated with the flow quantile bin of the flow $Q_{j.}$, and all other variables are as per equation 5.

4.1.1.2 Flow stratification with trend

We included a modified version of the flow stratification method to account for trends in water quality. This is useful when loads are required to be estimated for a particular point in time, rather than as an average over the complete observation period, particularly when there is a strong trend evident. We detrended the observation data by fitting Equation 12 to the concentration time series.

$$ln(\widehat{C_i}) = \beta_1 + \beta_2(t_i) \qquad \textit{(Equation 12)}$$

We then used the concentration residuals to develop a non-parametric rating curve. $\widehat{C}_j$ is calculated as the mean residual concentration associated with the flow quantile bin of the flow $Q_{j.}$, plus the predicted value of concentration at time T_j, which is multiplied by the smearing coefficient to account for the log transformation of Equation 12).

A3 Precision of load estimates

The statistical precision of a sample statistic, in this study the mean annual load, is the amount by which it can be expected to fluctuate from the population parameter it is estimating due to sample error. In this study, the precision represents the repeatability of the estimated load if it was re-estimated using the same method under the same conditions. Precision is characterised by the standard deviation of the sample statistic, commonly referred to as the standard error. We evaluated the standard error of each load estimate by bootstrap resampling (Efron, 1981). For each load estimate we constructed 100 resamples of the concentration data (of equal size to the observed dataset), each of which was obtained by random sampling with

replacement from the original dataset. Using each of these datasets, we recalculated the site load and estimated the 95% confidence intervals, using the boot r package. We represent precision in the results as the 95% confidence interval range, standardised by the load estimate (i.e., represented as a proportion).

A4 Selection of best load estimation methodology

TN loads were calculated for all sites using each of the four load estimation methods. We evaluated the performance of each rating curve method for predicting observed concentrations, using a range of model performance measures (see Fraser and Snelder (2019) for details). We identified site loads and method combinations that had any of:

1. large export coefficient values (i.e., site load divided by catchment area);

2. large differences in the loads calculated using different methods.

For these site and method combinations (approximately 10-20% of sites for each nutrient variable), we manually inspected diagnostic plots (e.g. C-Q plots, C-T plots, comparisons of sampled flow distributions relative to observed flow distributions). We used expert judgement to select the most appropriate load estimation method for each site that were outside of the two criteria outlined above. As well as selecting from one of the four rating curve methods described above, we also allowed sites to be discarded at this stage if no method appeared to satisfactorily describe the observed behaviour. This process also suggested that, for the manually inspected sites, the selection of the model with the lowest RMSD (in terms of performance in predicting observed concentrations) was the criteria most consistent with the outcomes of the expert judgement. For the remainder of the site and nutrient variable combinations that were not flagged by the above criteria (and for which the diagnostic plots were not inspected), the most appropriate load estimation method was selected as the rating curve method that yielded the lowest RMSD.

Appendix B   Point source load estimates in 2012 and 2017

Point Source Site Name	Load (kg/year)	
	2012	2017
AFFCO Fielding at Industrial Waste water	66940	47762
Ashhurst STP at Secondary oxpond waste	6364	1877
Bulls STP at Secondary oxpond waste	2673	2632
Dannevirke STP at microfiltered oxpond	55125	68217
DB Breweries at Industrial wastewater	1914	388
Eketahuna STP at Secondary oxpond waste	497	592
Feilding STP at Secondary oxpond waste	272778	302043
Fonterra Pahiatua wastewater	359	132
Foxton STP at Secondary oxpond waste	17227	16068
Halcombe at Secondary oxpond	1106	895
Hunterville STP at Microfiltration Plant	818	311
Kimbolton STP at oxpond waste	2147	1102
Longburn STP at oxpond waste	1085	572
Marton STP at Rock filtered oxpond waste	31755	31990
National Park STP at Secondary oxpond	2964	884
Norsewood STP at oxpond waste	890	716
NZ Pharmaceuticals wastewater	9150	0
Ohakea STP at Effluent outfall	3150	3595
Ohakune STP at Secondary oxpond waste	23565	28234
Ormondville STP at 2nd oxpond waste	242	205
Pahiatua STP at Tertiary oxpond waste	3278	2093
PNCC STP at Tertiary Treated Effluent	535542	579568
Pongaroa STP at 2nd oxpond waste	397	342
PPCS Oringi STP at oxpond waste	626	358
PPCS Shannon at Clarifier Effluent	54743	19675
Raetihi STP at Secondary oxpond waste	3324	3436
Rangataua STP at Secondary oxpond waste	176	187
Ratana STP at Secondary oxpond waste	793	524
Riverlands at Industrial wastewater	24812	28723
Rongotea STP at Secondary oxpond waste	4003	2804
Sanson STP at Secondary oxpond waste	4044	4318
Shannon STP at oxpond waste	51867	15797
Taihape STP at oxpond waste	7074	4672
Taumarunui STP at Tertiary treated waste	13171	14707
Tokomaru at oxpond waste	806	490
Waiouru STP at oxpond waste	23613	11699
Woodville STP at Secondary oxpond waste	1845	2262

Appendix C   Land use and export coefficient considerations

C1   Land use map

At the time of reporting, the best available land use data was HRC's 2008 land use map, which describes regional variation in land use in nine categories (Figure 7). Changes in total stock numbers between 2007 and 2012 (i.e., the baseline year) in the region were evaluated at the WMSZ level by Fraser and Snelder (2020). These data provide an indication of the change in land use intensity, and therefore, provide an indication of the potential difference in nitrogen emissions from land use between 2007 and 2012.

Data was available describing the number of animals in four stock type categories (dairy cows, beef cows, sheep and deer) that are collected on all enterprises involved in livestock farming by Statistics New Zealand as part of an annual agricultural production census (APC). Fraser and Snelder (2020) used these data to estimate the numbers of pastoral animals in each WMSZ and further modified these to indicate the land use intensity. To produce these measures, Fraser and Snelder (2020) used publicly available APC data, which are associated with a spatial layer comprising 960 hexagonal grid cells (35,000 ha) that cover all New Zealand (https://statisticsnz.shinyapps.io/livestock_numbers/). The grid cells were intersected with the polygons representing each WMSZ to evaluate the numbers of animals of each stock type in each zone in 2007 and 2012. The numbers of animals of each stock type were converted to 'stock units' which is a measure of metabolic demand that is commonly used in New Zealand (Parker, 1998). The stock units within each WMSZ were summed and divided by the area of the WMSZ to define the stock unit density (SU ha^{-1}) for 2007 and 2012. Differences in stock unit density between 2007 and 2012, expressed as percentages of 2012 density, were evaluated and used to represent change in land use intensity within each WMSZ.

The changes in stock unit density between 2007 and 2012 across the 124 WMSZs indicate that land use intensity generally decreased across the region (Table 6, Figure 22). Changes in land use intensity in either direction were less than 10% for 62% of the WMSZs and less than 20% for 91% of WMSZs (Table 6). The largest changes in land use intensity in relative terms occurred in WMSZs with the lowest levels of land use (Figure 22).

Table 6. Changes in land use intensity between 2007 and 2012 across the 124 WMSZs.

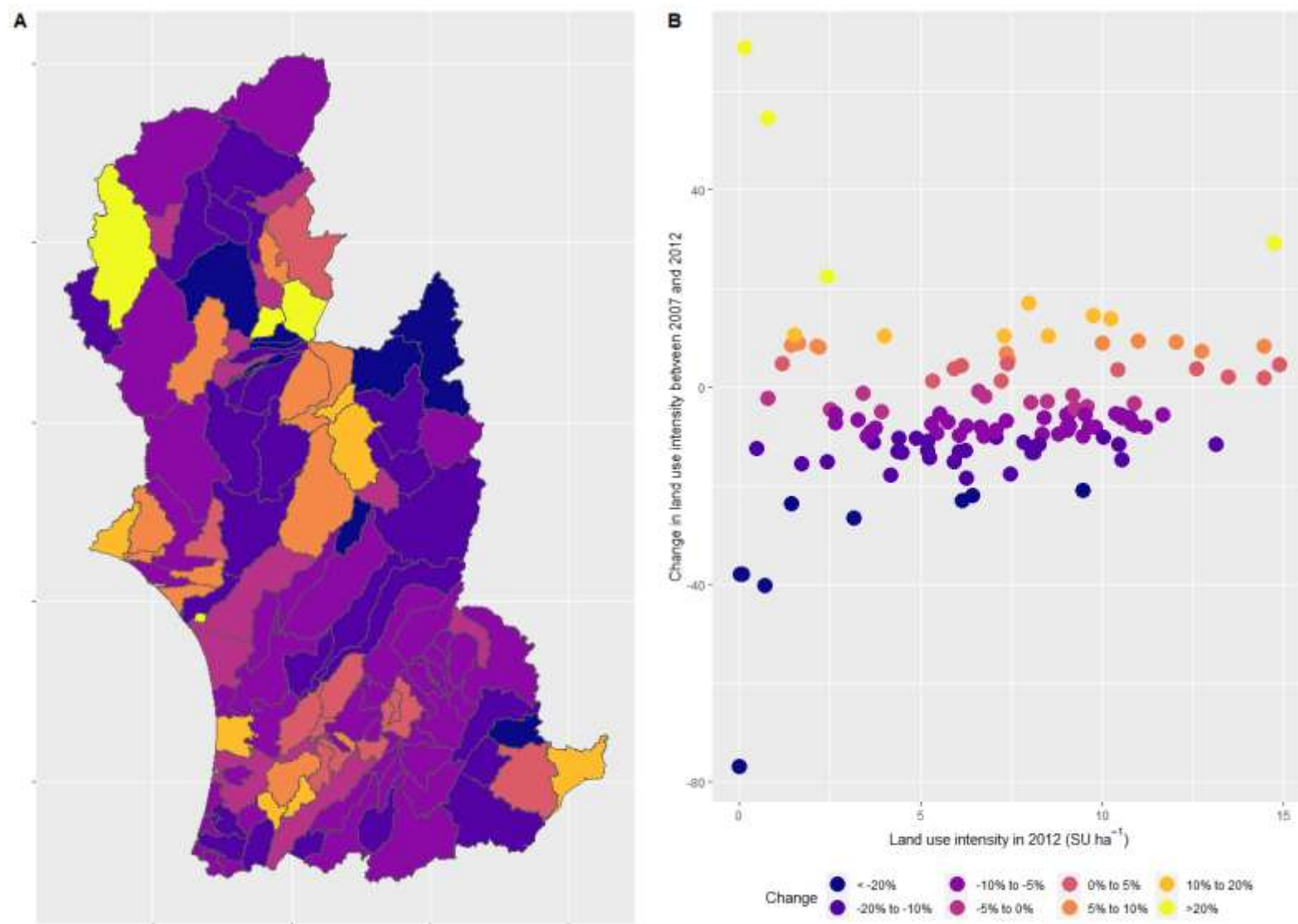| Change between 2007 and 2012 (%)	Proportion of WMZs (%)
< -20	7
-20 to -10	23
-10% to -5%	34
-5% to 0%	10
0% to 5%	9
5% to 10%	9
10% to 20%	6
>20%	3

Figure 22. Changes in stock unit density between 2007 and 2012 across the 124 WMSZs.

LWP

The changes in stock between 2007 and 2012 (total stock unit density SU ha^{-1}; Table 6, Figure 22) indicate that changes in land use intensity were generally less than 20% across all WMSZs. A proportion of these changes will have been changes of management on farms and therefore land use *per se* can be expected to have changed by less than this amount between 2007 and 2012. The land use pattern is relevant to the water quality models because it is used to estimate the magnitude of the diffuse source nitrogen export coefficients, which are discussed further below.

C2 Comparison of available export coefficient estimates

Export coefficients for a given farming operation vary depending on the characteristics of the farm. For example, climate and soils strongly influence nitrogen leaching losses, and, therefore, export coefficients are expected to vary in response to these factors. The available regionally-specific export coefficient estimates were either farm or catchment specific and did not allow us to account for variation in farm characteristics that occur at the regional scale. In contrast, the export coefficients defined by Bright *et al.* (2018) accounted for variation due to four biophysical factors including: climate zone, plant available soil water capacity (PAW), and whether the land is irrigable and irrigated. We therefore considered that the export coefficients defined by Bright *et al.* (2018) were the most appropriate estimates for this regional scale study but that the regionally-specific estimates made by other studies provided the opportunity to verify this decision. In the following section we compare the export coefficients that were used in this study (based on Bright *et al.*, 2018) with the available regionally specific estimates.

There were several regionally-specific sources of diffuse source nitrogen emission estimates from farms. First, the dairy farm consents database contains estimated nitrogen emissions from 211 dairy farms in the region based on their operations in 2012 and the OVERSEER nutrient budgeting model. Nitrogen emissions as export coefficients (i.e., kg N ha^{-1} yr^{-1}) were re-estimated for all farms in the database using version 6.2.2 of OVERSEER and the base files pertaining to 2012. This produced a set of export coefficients for the dairy farms that were consistent with the cumulative nitrogen leaching maximums in the updated One Plan Table 14 that is contained in Proposed Plan Change 2. Second, several studies have estimated average export coefficients from farms of different types (primarily sheep and/or beef and dairy) in different catchments within of the region (Collins *et al.*, 2017; Manderson, 2015; Singh and Elwan 2017).

We undertook a comparison of the estimated dairy farm export coefficients provided by the consents database with those defined by Bright *et al.* (2018) and those of Manderson *et al.* (2016) as reported by Singh *et al.* (2017). We first allocated the consents database farms to the same biophysical classes used by Bright *et al.* (2018), i.e. climate zone (Figure 8), a PAW category (Figure 9) irrigable (Figure 10) and irrigated (Figure 11). To do this we constructed a circular 800m buffer around the coordinates provided for each farm in the consents database (note that we did not have access to the farm boundaries). We chose 800m to emulate the mean area of the farms in the database of 200 ha. We intersected the buffer areas representing each farm with the spatial layers representing Climate zones, PAW, irrigable and irrigated areas. We allocated farms to a Climate, PAW, irrigable and irrigate category based on the dominant category of each layer within the buffered areas.

We then allocated all land in the region categorised as dairy land use (i.e., not just the dairy land represented in the consents database; Figure 7) to the stratification used by Bright *et al.* (2018). The relevant export coefficients defined by Bright *et al.* (2018) were assigned to all the strata in the region on which a dairy land use occurs and the area of dairy farms within each

strata were obtained. We then inspected the distribution of estimated nitrogen export coefficients for groups defined by the strata for the consents database, for all dairy land based on Bright *et al.* (2018) and rates estimated by Manderson *et al.* (2016).

The majority (71%) of the farms represented by the consents database were located within the South West Coast climate zone (Figure 8). The majority of all dairy farms are also located in the South West Coast climate zone (Figure 10). The remaining 14%, 8% and 7% of consented farms were in the Lower Hill Country, East Coast and Mountain climate zones. There were no consented farms in the North West climate zone and only a small proportion of all the dairy farms in the region were in this zone.

There was considerable variation in the export coefficients derived from the consents database even within climate zones, PAW and irrigation categories (Figure 23). The consents database export coefficients were, on average, lowest in the South West Coast climate zone. In the South West Coast climate zone, the central tendency of the consents database values were reasonably consistent with the median values of Manderson *et al.* (2016) as reported by (Singh *et al.*, 2017). The consistency within the South West Coast climate zone is expected because the dairy farms in the Rangitikei Catchment, on which the estimates of Manderson *et al.* (2016) were focussed, are mainly located within the South West Coast climate zone. Manderson *et al.* (2016) however reported a large range in the values and that level of variation was reasonably consistent with the variation in the values derived from the consents database. In the other climate zones, the majority of export coefficients derived from the consents database and Bright *et al.* (2018) were within the range of Manderson *et al.* (2016). The export coefficients derived from Bright *et al.* (2018) were generally reasonably consistent with those derived from the consents database (i.e., were generally within the interquartile range). The export coefficients derived from *Bright et al.* (2018) were always higher than the median values of Manderson *et al.* (2016) but were always within range of values except for one strata in the South West Coast zone.
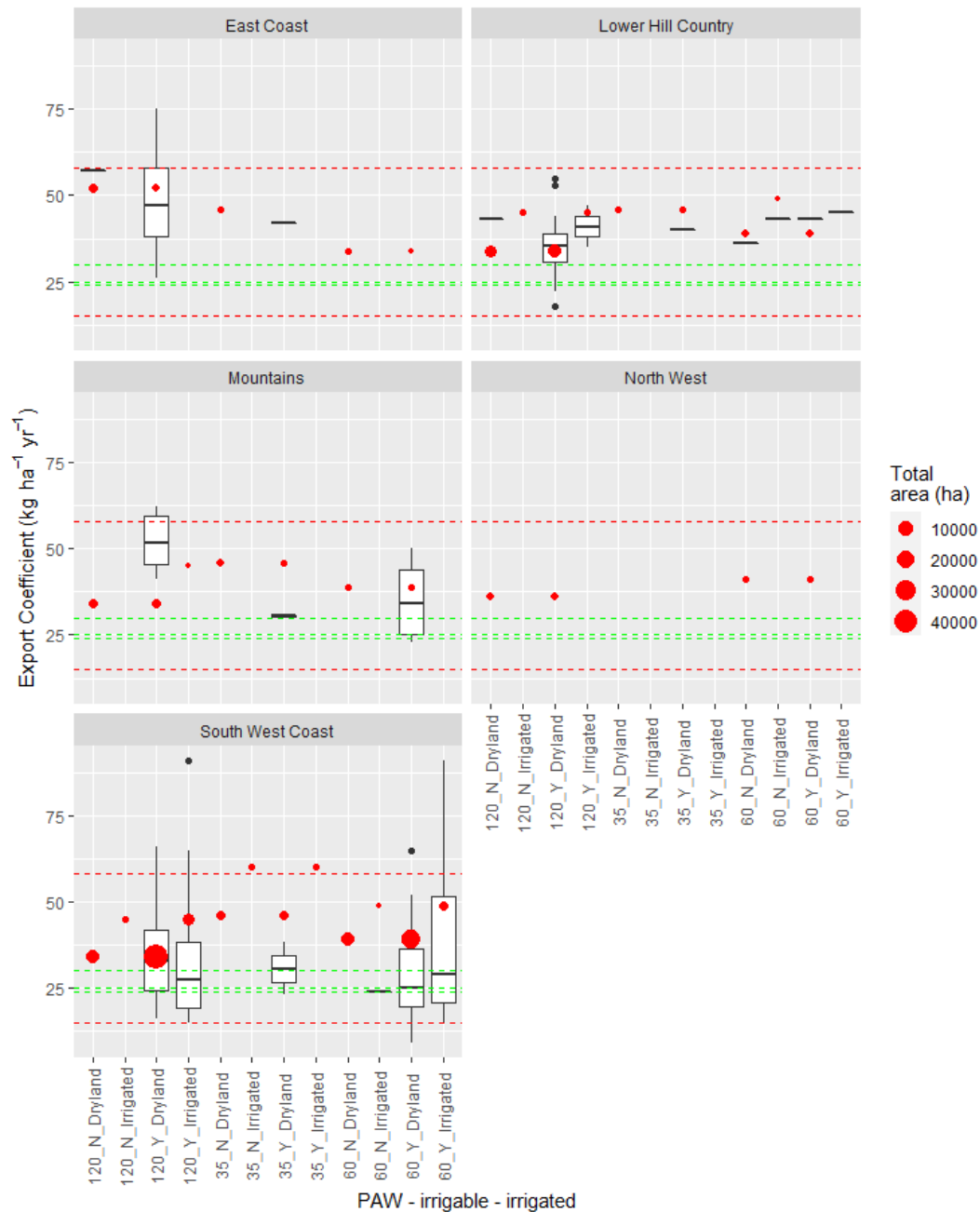
Figure 23. Comparison of diffuse source export coefficients for dairy farms provided from a range of sources within each strata (i.e., Climate, PAW, irrigable and irrigate categories) used by Bright et al. (2018). The box and whisker plots show the distributions of nitrogen leaching rates estimated for farms in the consents database. The box indicates the inter-quartile range and the horizontal bar within the box indicates the median. The whiskers indicate the lowest datum still within 1.5 IQR of the lower quartile, and the highest datum still within 1.5 IQR of the upper quartile. Outliers are indicated by black dots. The red dots show the equivalent rates defined by Bright et al. (2018). The dots are scaled to represent the total area of dairy farms in the region. The red dashed lines indicate the lower and upper bounds and the green dashed lines represent the median for low, medium and high intensity of dairy farm loss rates reported for the Rangitikei catchment by Manderson et al. (2016) as reported by (Singh et al., 2017). Note that dairy farms having some combinations of climate and PAW categories are not represented by any farm in the consents database.

We undertook a comparison of export coefficients for sheep and beef farming defined by Bright *et al.* (2018) with those estimated for the Mangatainoka catchment by Manderson (2015) and the Rangitikei catchment by Manderson *et al.* (2016). Manderson (2015) estimated export coefficients for sheep and beef farms in the Mangatainoka catchment using three methods. Methods 1 and 3 considered many farms but omitted consideration of farm management practice. These methods produced rates between 9.6 kg ha^{-1} yr^{-1} to 12.2 kg ha^{-1} yr^{-1}. Method 2 was based on a more detailed consideration of a small number of farms on different types of terrain. The method produced higher N loss estimates of 20.2 kg ha^{-1} yr^{-1}, which reduced to 17 kg ha^{-1} yr^{-1} when an annual rainfall of 1300 mm yr^{-1} was assumed. This lower rainfall is consistent with the lower catchment and is within the South West Coast climate zone (Figure 8). Manderson (2015) suggested a "best" estimate of the export coefficient of 12.9 kg ha^{-1} yr^{-1}, which was based on combining the strengths of Method 1 (large sample and strong extrapolation) with those of Method 2 (inclusion of farm management effects). Sheep and beef farming export coefficients for the Rangitikei catchment derived by Manderson *et al.* (2016) are reported by Singh *et al.* (2017). The export coefficients were estimated at between 9 kg ha^{-1} yr^{-1} and 10.5 kg ha^{-1} yr^{-1} under sheep and beef grazing and the range was between 5 kg ha^{-1} yr^{-1} and 18 kg ha^{-1} yr^{-1} depending on the farming intensity.

We allocated all land in the region categorised as sheep and beef land use to the stratification used by Bright *et al.* (2018). The relevant export coefficients defined by Bright *et al.* (2018) were assigned to all the strata in the region on which sheep and beef use occurs and the area of farms within each strata were obtained. We then compared estimated nitrogen export coefficients for groups defined by the strata based on Bright *et al.* (2018) and rates estimated by Manderson (2015) and Manderson *et al.* (2016).

The export coefficients estimated by Bright *et al.* (2018) were higher than those of Manderson (2015) and Manderson *et al.* (2016) for all climate zones except Mountains (Figure 24). The largest deviations between the estimates were associated with irrigated sheep and beef farms. This is probably because the estimates of Manderson (2015) and Manderson *et al.* (2016) were based only on dryland farms. The analysis indicated that irrigated sheep and beef farms made up only a small proportion of the total land used for sheep and beef farming (Figure 24). For the Mountains climate zone, the export coefficients estimated by Bright *et al.* (2018) were significantly lower than the Manderson estimates. The Bright *et al.* (2018) estimates for the South West Coast climate zone were most consistent with the best estimate of Manderson *et al.* (2016). This consistency is logical because Manderson *et al.'s* (2016) estimates were focussed on farms that are mainly located within the South West Coast climate zone.
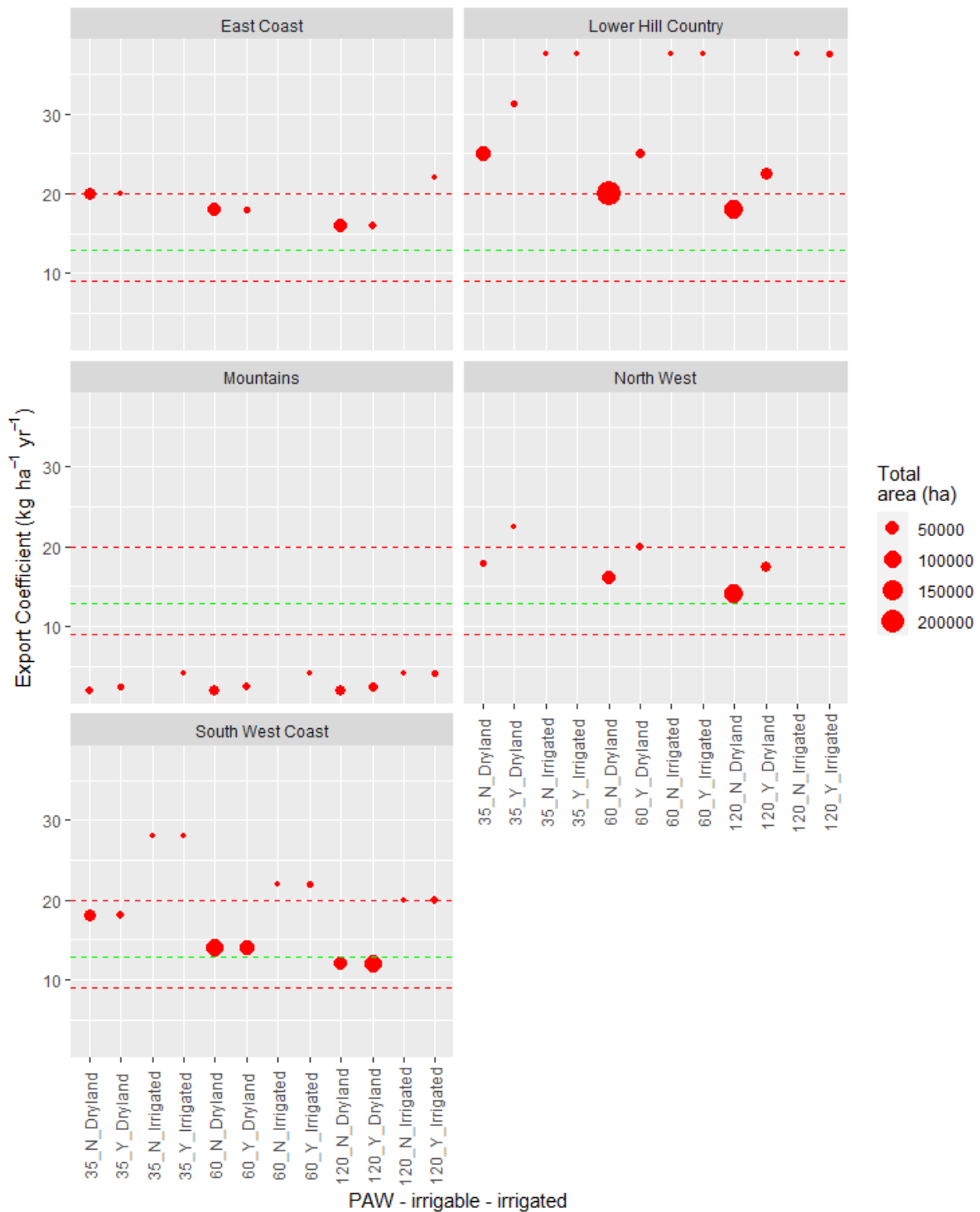
Figure 24. Comparison of diffuse source export coefficients for sheep and beef farms within each strata (i.e., Climate, PAW, irrigable and irrigate categories) used by Bright et al. (2018). Export coefficients for sheep and beef farms defined by Bright et al. (2018) are shown as red dots. The dots are scaled to represent the total area of sheep and beef farms in the region. The best estimate of Manderson (2015) for the Mangatainoka catchment (green dashed line) and the range in estimates of Manderson et al. (2016) for the Rangitikei Catchment (red dashed lines).

The analysis of nitrogen loss rates detailed in the dairy consents database, previous studies and adopted in this study based on Bright *et al.* (2018), show that there is a reasonably high level of consistency in the central tendency of the various estimates but that there is also considerable range in plausible nitrogen export coefficients. This indicates that the export coefficients that are key input data to the water quality models are highly uncertain. Taken together, the uncertainties in the model input data (i.e., land use map and export coefficients) mean that potential differences in model predictions resulting from the non-congruence of dates for the land use and catchment nitrogen emission estimates are unlikely to be statistically significant (i.e., any differences would be within the model uncertainty). In addition, the water quality models are calibrated to water quality station nitrogen loads, which are themselves uncertain (Figure 22). These uncertainties are all compounded in the models and mean our confidence is highest when the model is used to predict the relative difference in water quality outcomes between two scenarios. A formal analysis of the model uncertainty and assessment of possible differences due to land use changes is possible with the CASM models but was beyond the scope of this study.